European Journal of Medicinal Chemistry 157 (2018) 1376–1394

Contents lists available at ScienceDirect

European Journal of Medicinal Chemistry

journal homepage: http://www.elsevier.com/locate/ejmech

Research paper

Structure-activity and structure-property relationships of novel Nrf2 activators with a 1,2,4-oxadiazole core and their therapeutic effects on acetaminophen (APAP)-induced acute liver injury

Li-Li Xu [a, b, c], Yu-Feng Wu [c], Lei Wang [a, b], Cui-Cui Li [c], Li Li [a, b], Bin Di [c, ***], Qi-Dong You [a, b, **], Zheng-Yu Jiang [a, b, *]

[a] State Key Laboratory of Natural Medicines and Jiangsu Key Laboratory of Drug Design and Optimization, China Pharmaceutical University, Nanjing, 210009, China
[b] Department of Medicinal Chemistry, School of Pharmacy, China Pharmaceutical University, Nanjing, 210009, China
[c] Key Laboratory on Protein Chemistry and Structural Biology, Key Laboratory of Drug Quality Control and Pharmacovigilance, Ministry of Education, China Pharmaceutical University, Nanjing, 210009, China

ARTICLE INFO

Article history:
Received 22 May 2018
Received in revised form
11 August 2018
Accepted 25 August 2018
Available online 28 August 2018

Keywords:
Nrf2 activators
Oxadiazole core
Acute liver injury
Structure-activity relationship
Antioxidant function

ABSTRACT

The antioxidant function induced by Nrf2 protects the liver from damage. We found a novel Nrf2 activator named compound **25** via structural modification of compound **1** we previously reported. *In vitro*, compound **25** induced Nrf2 transport into the nucleus and protected hepatocyte L02 cells from APAP-induced cytotoxicity via activating the Nrf2-ARE signaling pathway. *In vivo*, **25** exhibited therapeutic effects in a mouse model of acute liver injury induced by acetaminophen (APAP) by up-regulating Nrf2-dependent antioxidases and down-regulating liver injury markers in serum. Together, these results indicated that **25** is a potent Nrf2/ARE activator both *in vitro* and *in vivo*. The drug-like properties of compound **25** further revealed its potential for development as a therapeutic drug against acute liver injury.

1. Introduction

It is generally thought that the induction of nuclear factor erythroid 2 p45-related factor 2 (Nrf2) to resist environmental stress is a promising strategy for maintaining cellular homeostasis [1,2]. Nrf2, as a member of the basic-leucine zipper (b-ZIP) transcription factor family [3], plays a critical role in antioxidant stress [4,5]. In a stress-free state, Nrf2 is anchored in the cytoplasm by kelch-like ECH-associated protein 1 (Keap1) and is directed toward ubiquitin-mediated proteasomal degradation [6,7]. This process maintains intracytoplasmic Nrf2 at a low level [8,9]. When cells are exposed to oxidative stress, such as reactive oxygen species (ROS), the cysteine residues of Keap1 are oxidized or alkylated resulting in structural changes in Keap1 [10,11]. Nrf2 detaches from Keap1 for stabilization and is no longer ubiquitinated and degraded [12,13]. Meanwhile, the newly synthesized Nrf2 accumulates and translocates into the nucleus and then forms heterodimers with small Maf proteins [8,14]. The heterodimer binds to the antioxidant response element (ARE), participating in the regulation of antioxidant enzymes including NAD(P)H: quinone oxidoreductase-1 (NQO1), hemeoxygenase-1 (HO-1) and γ-glutamylcysteine (γ-GCS) [15,16].

The liver is the first organ through which oral xenobiotics pass after being absorbed by the intestine and is the primary site of

* Corresponding author. State Key Laboratory of Natural Medicines and Jiangsu Key Laboratory of Drug Design and Optimization, China Pharmaceutical University, Nanjing, 210009, China.
** Corresponding author. State Key Laboratory of Natural Medicines and Jiangsu Key Laboratory of Drug Design and Optimization, China Pharmaceutical University, Nanjing, 210009, China.
*** Corresponding author. Key Laboratory on Protein Chemistry and Structural Biology, Key Laboratory of Drug Quality Control and Pharmacovigilance, Ministry of Education, China Pharmaceutical University, Nanjing, 210009, China.
E-mail addresses: dibin@cpu.edu.cn (B. Di), youqd@163.com (Q.-D. You), jiangzhengyucpu@163.com (Z.-Y. Jiang).

https://doi.org/10.1016/j.ejmech.2018.08.071
0223-5234/

bioconversion and metabolism [17]. Oxidative stress is associated with liver diseases including fibrosis, cirrhosis and advanced hepatocellular carcinoma (HCC) [18]. Therefore, reducing oxidative stress plays a critical role in the treatment of liver diseases [19]. Thus, the antioxidant function of Nrf2 activation has been extensively studied in the treatment of liver diseases [20–22]. Nrf2-knockout and Keap1-knockout mouse models have been used to study the protective function of Nrf2 activation [23,24]. Nrf2 can act as a research target in the prevention and treatment of liver diseases [25,26].

Acetaminophen (APAP) is the most common drug that causes drug-induced liver damage clinically. After APAP is absorbed by the body, 90% of APAP is excreted in combination with glucuronic acid or sulfuric acid. The remaining 5%–10% of APAP is metabolized by the cytochrome p450 (CYP450) system. APAP is metabolized to produce n-acetyl-para-benzoquinone imine (NAPQI). The toxic metabolite NAPQI is detoxified by glutathione (GSH) [27]. Once GSH is depleted in hepatocytes, NAPQI reacts with the sulfhydryl groups of protein to form an NAPQI-protein adduct. The formation of protein adducts is a key initiation event leading to hepatotoxicity [28].

Many studies suggest that APAP-induced liver injury can trigger the compensatory activation of Keap1-Nrf2 signaling pathway *in vivo*. The possible mechanisms are as follows: 1. NAPQI depletes GSH in hepatocytes to produce oxidative stress. 2. NAPQI directly modifies the cysteine thiol groups of Keap1 in the cytoplasm to alter the conformation of Keap1 and to disrupt the Keap1-Nrf2 interaction. Nrf2 is dissociated from Keap1 and translocated into the nucleus. The above two factors work together to activate the Nrf2 pathway. Nrf2 binds to ARE in the nucleus and promotes the expression of detoxification-related target proteins including NQO1, cysteine ligase catalytic subunit (GCLC) and cysteine ligase regulatory subunit (GCLM) for detoxification. This is also a self-protection mechanism of the body [29–31].

We previously reported a novel Nrf2 activator known as compound **1**, which has a *p*-fluorine in the phenyl group (ring A). We also systematically studied the structure–activity relationship (SAR) of ring A [32]. To obtain more potential candidate compounds and further improve the structure-activity relationship, we performed a more comprehensive structural modification of the rings A and C. In this paper, **1** was chosen as the initial compound. To further assess the effect of halogen substituents on ring A, we focused on changes in ARE-inducing activity when phenyl group was introduced into halogen substituents including −F, −Cl and −Br in various combinations. Sixteen compounds were synthesized and evaluated using the ARE-luciferase reporter gene assay. Among them, compound **6**, bearing two −F substituents at the meta and para positions of phenyl group, exhibited enhanced ARE-inducing activity as compared with **1**. Therefore, retaining this privileged structure fragment, the subsequent structural modifications were primarily focused on ring C. Twenty-five compounds were synthesized. The results revealed that **25** with ring C replaced by 3′4-methylpyridinyl was the most potent Nrf2 activator, presenting enhanced ARE-inducing activity and improved physicochemical properties (4-fold increase in intrinsic solubility compared to compound **1**). Further assessments of its biological activity indicated that in normal liver cells (L02), **25** promoted the nuclear translocation of Nrf2 and increased the expression of Nrf2-driven downstream antioxidant proteins including NQO1 and HO-1. Even at high concentrations, compound **25** did not show significant cytotoxicity in L02 cells. Moreover, **25** showed *in vivo* therapeutic effects in an APAP-induced acute liver injury mouse model by activating the Nrf2-ARE pathway. Compound **25** induced the up-regulation of antioxidant proteins and the down-regulation of hepatic injury markers in serum. These results demonstrated that **25** would be a potent Nrf2/ARE activator and a liver protective agent.

2. Results

2.1. Structure-activity relationship study of derivatives containing a 1,2,4-oxadiazole core

2.1.1. Design, synthesis and evaluation of ring A derivatives

In our previous research, compound **1** with a *p*-fluorine substituent in phenyl A exhibited optimal ARE-inducing activity [32]. In this paper, compound **1** was selected as the starting compound for further structural modifications and SAR studies. The changes in ARE-inducing activity deserved attention when ring A was introduced to multiple halogen substituents including −F, −Cl and −Br (Fig. 1). We synthesized sixteen compounds **1**–**16** and evaluated their Nrf2-ARE inducing activities using the ARE-luciferase reporter gene assay. Dimethyl fumarate (DMF) [33] and tertiary butylhydroquinone (*t*BHQ) [34] were used as positive controls (Table 1). The synthesis route of these derivatives is summarized in Scheme 1.

The Nrf2-ARE inducing activities of all the synthetic derivatives with halogen substituents in ring A were evaluated in stably transfected HepG2-ARE-C8 cells using the ARE-luciferase reporter gene assay. The position of the −F substituent in the phenyl ring was crucial to the activity of these compounds. Among them, when ring A was substituted with a single −F, the derivative with the −F substituent at the para position (**1**) was the most active compound, followed by derivatives with ortho (**4**) or meta (**5**) position occupied by −F. When the para-position of ring A was substituted with a single substituent of −F, −Cl or −Br, the derivative with a −F substituent at the para position (**1**) was the most active compound, followed by those with −Cl (**2**) and −Br (**3**) substituents at the para position. In summary, the charge and position of the substituents could influence the ARE-inducing activity. When ring A was switched with a single halogen substituent, −F was preferred as the para substituent.

Next, we investigated changes in the ARE-inducing activity of the derivatives when two halogen substituents were introduced into ring A. When the para position of the ring A was occupied by the −F element, the −F, −Cl or −Br substituents were introduced into the meta position. The ARE-inducing activities of those derivatives showed that **6** with two −F substituents in the para and meta positions of phenyl (3, 4-F) was the most active compound. In addition, the para position of ring A was also occupied by the −F substituent, and the substituents −F, −Cl or −Br were introduced into the ortho position. The ARE-inducing activity for 2-Br-4-F (**13**) was stronger than that for 2-Cl-4-F (**8**) and 2, 4-F (**10**). Among these derivatives, **6** (*m*, *p*-F) showed concentration-dependent Nrf2-ARE inducing activity and was more potent than **1** (*p*-F). However, when ring A was introduced to three substituents, the ARE-inducing activities of the compounds decreased significantly.

2.1.2. Design, synthesis and evaluation of ring C derivatives

Among the ring A derivatives, **6** with *m*, *p*-F substituents in phenyl A showed potent ARE-inducing activity. We subsequently performed modifications of ring C to obtain twenty-five derivatives while maintaining ring A as an *m*, *p*-F substituted benzene ring. During this process, the benzo[*d*]imidazole group (ring C) was replaced with multiple types of heterocyclic substituents or phenyl (Fig. 1). The synthesis route of these derivatives is summarized in Scheme 2.

The Nrf2-ARE inducing activities of all ring C derivatives in HepG2-ARE-C8 cells were evaluated using the ARE-luciferase reporter gene assay and summarized in Table 2. Compound **25** (3′4-methylpyridinyl) at 80 μM exerted an optimal induction activity of 59.55-fold compared to the blank control, which was superior to **1** and **6** at the same concentration. The ARE-inducing activity was decreased when ring C (benzo[*d*]imidazole group) was replaced

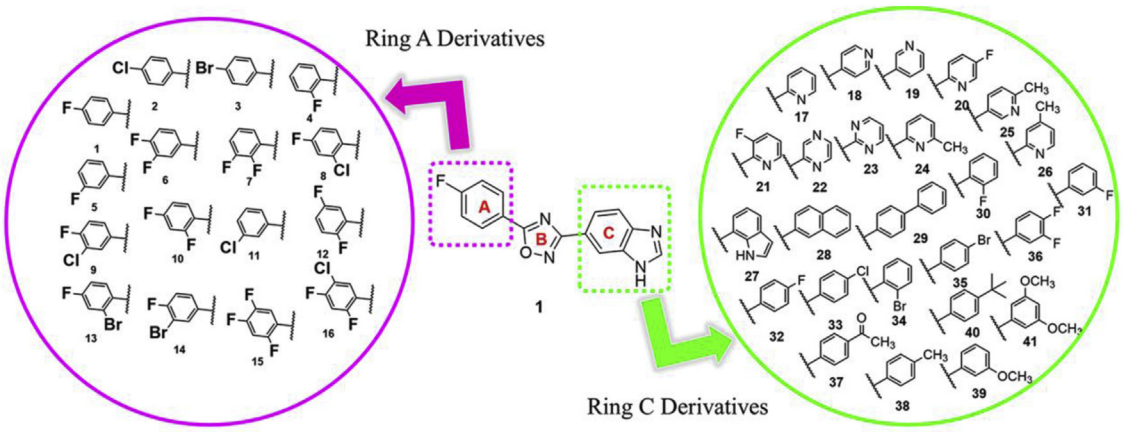

Fig. 1. The structures of the derivatives containing a 1,2,4-oxadiazole core.

Table 1
Nrf2-inducing activity of sixteen derivatives containing a 1,2,4-oxadiazole core and halogen substituents measured using the luciferase reporter gene assay.

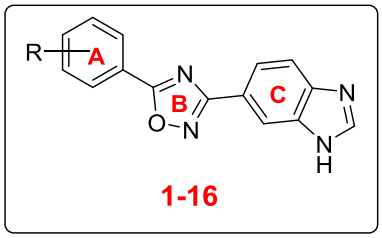

Cpd.	R	ARE-inducing activity in luciferase reporter assay (μM)[a,b]					
		0.01	0.1	1	20	40	80
1	**4-F**	1.57 ± 0.29	2.49 ± 0.67	10.23 ± 0.66	27.28 ± 1.26	40.81 ± 0.22	44.40 ± 0.89
2	**4-Cl**	0.33 ± 0.05	0.72 ± 0.06	1.64 ± 0.18	15.49 ± 1.03	18.52 ± 0.98	14.14 ± 0.49
3	**4-Br**	0.22 ± 0.02	0.25 ± 0.05	0.87 ± 0.12	13.41 ± 0.72	3.44 ± 1.51	2.75 ± 0.15
4	**2-F**	2.01 ± 0.24	4.51 ± 0.30	12.04 ± 1.50	12.70 ± 2.90	15.04 ± 1.60	19.09 ± 1.01
5	**3-F**	1.21 ± 0.44	2.69 ± 0.29	4.49 ± 2.79	8.83 ± 1.33	12.38 ± 2.01	14.10 ± 1.12
6	**3,4-F**	1.46 ± 0.18	6.21 ± 0.68	12.35 ± 0.51	24.03 ± 0.80	42.61 ± 2.43	49.86 ± 0.30
7	**2,3-F**	1.77 ± 0.18	2.22 ± 0.18	3.70 ± 0.17	4.55 ± 0.12	10.69 ± 1.80	16.51 ± 4.11
8	**2-Cl-4-F**	0.68 ± 0.15	2.98 ± 0.12	4.22 ± 1.28	11.8 ± 0.36	14.71 ± 0.42	18.31 ± 2.05
9	**3-Cl-4-F**	1.04 ± 0.28	3.88 ± 0.34	3.22 ± 0.24	7.53 ± 0.05	9.59 ± 0.25	12.49 ± 0.21
10	**2,4-F**	1.62 ± 0.18	2.17 ± 0.47	2.48 ± 0.48	4.58 ± 0.46	7.34 ± 0.61	8.36 ± 0.58
11	**3-Cl**	1.74 ± 0.08	3.23 ± 0.37	4.78 ± 0.34	12.79 ± 1.01	13.19 ± 0.21	19.15 ± 0.70
12	**2,5-F**	2.31 ± 0.01	4.15 ± 1.35	5.24 ± 0.02	16.85 ± 1.21	20.20 ± 1.46	21.87 ± 2.70
13	**2-Br-4-F**	1.01 ± 0.13	2.65 ± 0.02	4.18 ± 1.48	12.10 ± 0.06	21.59 ± 0.61	25.15 ± 0.41
14	**3-Br-4-F**	1.68 ± 0.21	1.36 ± 0.44	1.89 ± 0.09	3.46 ± 0.22	3.92 ± 0.64	4.84 ± 0.98
15	**2,4,5-F**	1.55 ± 0.59	1.86 ± 0.51	2.15 ± 1.29	3.95 ± 0.09	4.36 ± 0.04	7.92 ± 1.56
16	**5-Cl-2,4-F**	1.94 ± 0.38	1.18 ± 0.32	1.26 ± 0.16	3.35 ± 1.23	5.14 ± 0.64	7.61 ± 0.63
DMF		0.82 ± 0.04	1.00 ± 0.07	1.10 ± 0.08	1.65 ± 0.35	2.97 ± 0.45	ND
		0.02	**0.2**	**2**	**20**	**40**	**80**
***t*BHQ**		1.18 ± 0.08	1.25 ± 0.01	1.24 ± 0.04	1.41 ± 0.07	2.14 ± 0.10	5.27 ± 0.41

[a] The inducing activity of the compound was calculated compared to the blank control, and the data are presented as the mean ± SEM of three separate experiments.
[b] All compounds showed no significant anti-proliferative effects at the concentration of 80 μM.

with pyridine (**17**, **18**, **19**), pyrazine (**22**) and pyrimidine (**23**) compared to that of **1**. In addition, the ARE-inducing activity decreased when the −F substituent was imported into pyridine (**20**, **21**) compared with that of **1**. However, the replacement of the benzo[*d*]imidazole group with (3′4-methylpyridinyl) (**25**) enhanced the ARE-inducing activity compared to that of **1**. In contrast, the ARE-inducing activity was significantly reduced when the benzo[*d*]imidazole group was substituted with 2′3-methylpyridinyl (**24**) and 2′5-methylpyridinyl (**26**). This result showed that the position of the methyl substituent on pyridine played an important role in maintaining its activity. Substitution of the benzo[*d*]imidazole group with an indole ring (**27**), naphthalene ring (**28**) and biphenyl (**29**) also resulted in a decrease in ARE-inducing activity compared with that of **1**. Next, we explored the change in ARE-inducing activity when the benzo[*d*]imidazole group was replaced with phenyl. The para position of the benzene ring was replaced with electron-donating groups, including $-CH_3$ (**38**), $-OCH_3$ (**39**), and −tertiary butyl (**40**) or weak electron-withdrawing substituent of −Br (**35**), which were superior to the strong electron-withdrawing substituents, including −F (**30**, **31**, **32**), −Cl (**33**) and −acetyl (**37**). Unlike ring A, the introduction of electron-donating groups to ring C promoted the Nrf2-ARE

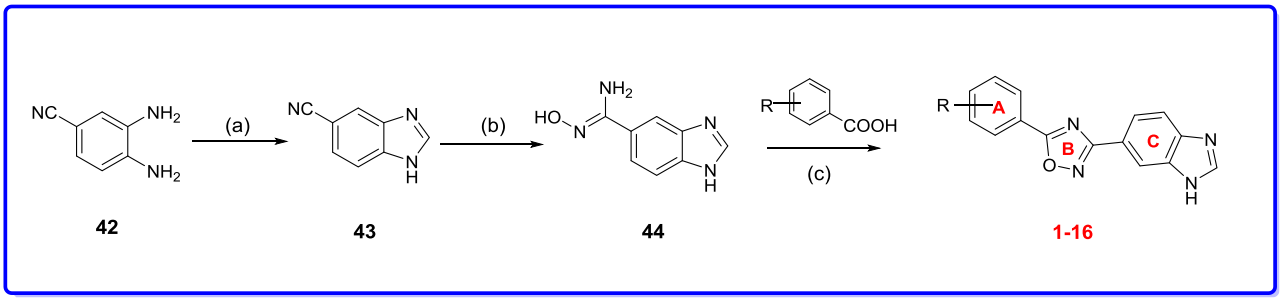

Scheme 1. Synthetic route of 1,2,4-oxadiazole derivatives with halogen substituents.
Reagents and conditions: (a) 5 M HCl, HCOOH, reflux, 4 h, 94%; (b) K_2CO_3, EtOH, $H_2NOH{\cdot}HCl$, reflux, 12 h, 50%; (c) CDI, DMF, 110 °C, 12–18 h.

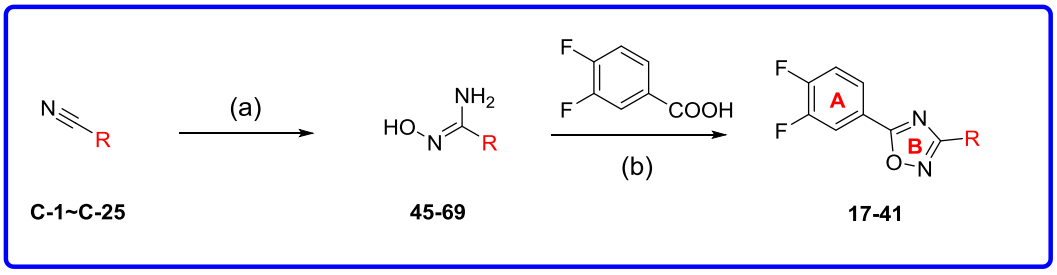

Scheme 2. Synthetic route of 1,2,4-oxadiazole derivatives of ring C.
Reagents and conditions: (a) K_2CO_3, EtOH, $H_2NOH{\cdot}HCl$, reflux, 12 h; (b) CDI, DMF, 110 °C, 12–18 h.

inducing activity, while electron-withdrawing groups decreased this activity. Meanwhile, no substitution or multiple substitutions in ring C impaired the Nrf2-ARE inducing activity.

In summary, the SAR studies could be described as follows: (1) For phenyl ring A replaced with a single halogen substituent, the introduction of para-F up-regulated the Nrf2-ARE inducing activity. (2) When two halogen substituents were introduced into phenyl ring A and the para position was replaced with −F, the meta position was preferential to −F (3−F) and the ortho position was preferential to −Br (2−Br). (3) Introduction of three substituents into ring A significantly decreased the ARE-inducing activity. (4) When ring C was replaced with phenyl and nitrogen-containing heterocyclic rings, the introduction of electron-donating substituents into ring C promoted the Nrf2-ARE inducing activity, while electron-withdrawing substituents impaired this activity. (5) The ARE-inducing activity decreased when ring C was replaced with phenyl having zero or multiple substituents.

2.2. Physicochemical properties of the active compounds

To identify potential drug-like compounds, we determined the physicochemical properties of several compounds that exhibited potent ARE-inducing activity using the luciferase reporter gene assay. Log*D* (pH 7.4) and intrinsic aqueous solubility were determined on the Gemini Profiler instrument (pION) by the "gold-standard" Avdeef-Bucher potentiometric titration method. As shown in Table 3, although the log$D_{7.4}$ values remained the same, the solubilities of all the selected compounds changed significantly. Among them, the intrinsic solubility of **25** (250 μM) was optimal, which was 4 times that of compound **1** (intrinsic solubility was 66.90 μM) and 2.5 times that of compound **6** (intrinsic solubility was 99 μM). The introduction of hydrophilic groups such as 3′4-methylpyridinyl (**25**), 2′3-methylpyridinyl (**24**) and 2′5-methylpyridinyl (**26**) significantly improved the solubility. The introduction of hydrophobic substituents including biphenyl (**29**), benzyl (**38**) and benzene ring with methoxyl groups (**39**) rendered poor solubility. Taken together, compound **25**, which presented potent ARE-inducing activity and appropriate physicochemical properties, was selected for further pharmacological studies.

2.3. Pharmacological results

2.3.1. Cytotoxicities of the selected derivatives

For compounds having excellent Nrf2-ARE inducing activity in the luciferase reporter gene assay, the normal liver cell line L02 was selected to test for cytotoxicity by the MTT method. L02 cells were treated with derivatives (Fig. 2) having potent ARE-inducing activities for 24 h at concentrations of 0.2, 2, 20, 40, 80 and 160 μM. *t*BHQ was used as the positive control. Compound **25** and *t*BHQ exhibited no more than 7% cytotoxicity even at concentrations up to 160 μM. Compounds **1** and **6** showed no more than 20% cytotoxicity in L02 cells at the high concentration of 160 μM.

2.3.2. Effects of **25** on the Nrf2-ARE pathway

Nrf2, which escapes ubiquitin degradation, can translocate into the nucleus and bind to ARE, resulting in the up-regulation of Nrf2-dependent downstream markers. We investigated the modulation of **25** on Nrf2 and Nrf2-dependent proteins including NQO1 and HO-1 in L02 cells. Compound **25** increased the protein expression of NQO1, HO-1 and Nrf2 in L02 cells in time-dependent and concentration-dependent manners (Fig. 3A and B). To confirm that the up-regulation of downstream antioxidant proteins was caused by Nrf2 activation, siRNA was designed to purposefully down-regulate the Nrf2 mRNA transcription. The qRT-PCR results showed that when the Nrf2 gene transcription level was purposefully down-regulated to 30% by Nrf2 siRNA, the mRNA transcriptions of NQO1, GCLM and HO-1 were also down-regulated. The addition of **25** (20 μM) obviously up-regulated the mRNA transcription levels of Nrf2 and its downstream genes including NQO1, GCLM and HO-1 (Fig. 3C and 3E). The above results indicated that

Table 2
Nrf2-inducing activity of ring C derivatives containing a 1,2,4-oxadiazole core as determined by the luciferase reporter gene assay.

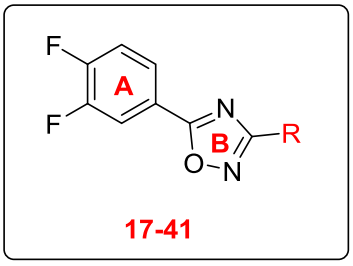

Cpd.	R	ARE–inducing activity in luciferase reporter assay (μM)[a,b]					
		0.01	0.1	1	20	40	80
1	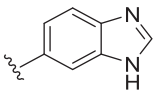	1.57 ± 0.29	2.49 ± 0.67	10.23 ± 0.66	27.28 ± 1.26	40.81 ± 0.22	44.40 ± 0.89
6	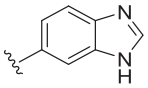	1.46 ± 0.18	6.21 ± 0.68	12.35 ± 0.51	24.03 ± 0.81	42.61 ± 2.43	49.86 ± 0.31
17	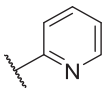	0.65 ± 0.35	0.83 ± 0.02	1.05 ± 1.35	1.31 ± 0.14	1.32 ± 0.42	2.55 ± 0.07
18	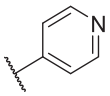	1.08 ± 0.26	1.62 ± 0.67	1.07 ± 0.31	1.29 ± 0.47	1.72 ± 0.07	2.88 ± 0.86
19	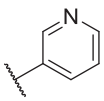	1.45 ± 0.91	1.71 ± 0.70	2.02 ± 0.70	3.15 ± 1.20	3.15 ± 0.49	4.15 ± 0.35
20	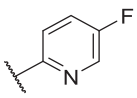	0.96 ± 0.30	1.97 ± 0.31	2.17 ± 0.07	2.95 ± 0.84	5.79 ± 0.90	6.35 ± 0.98
21	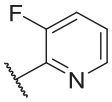	1.15 ± 0.14	1.25 ± 0.07	1.56 ± 0.14	1.75 ± 0.07	2.52 ± 0.56	2.95 ± 0.21
22	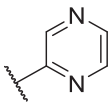	1.13 ± 0.33	1.43 ± 0.40	1.95 ± 0.07	1.81 ± 0.01	2.83 ± 0.84	3.35 ± 0.38
23	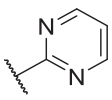	0.92 ± 0.31	1.06 ± 0.26	1.07 ± 0.53	2.05 ± 0.35	2.95 ± 0.49	5.82 ± 0.74
24	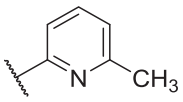	1.16 ± 0.38	1.08 ± 0.01	2.65 ± 0.81	3.96 ± 1.14	4.46 ± 0.68	5.68 ± 0.14
25	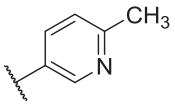	2.75 ± 0.21	3.46 ± 0.28	16.1 ± 0.98	24.66 ± 0.14	48.73 ± 0.28	59.55 ± 0.49
26	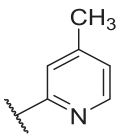	0.63 ± 0.11	1.06 ± 0.02	2.04 ± 0.51	8.96 ± 0.44	9.76 ± 0.28	10.58 ± 0.14

Table 2 (*continued*)

Cpd.	R	ARE–inducing activity in luciferase reporter assay (μM)[a,b]					
		0.01	0.1	1	20	40	80
27	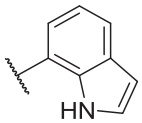	0.83 ± 0.31	1.88 ± 0.47	2.01 ± 0.01	2.36 ± 0.17	3.77 ± 0.38	4.02 ± 0.35
28	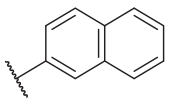	1.16 ± 0.12	1.27 ± 0.21	1.52 ± 0.35	1.96 ± 0.30	1.96 ± 0.35	3.57 ± 0.49
29	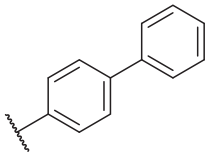	1.15 ± 0.07	1.25 ± 0.35	6.75 ± 0.38	8.54 ± 1.18	10.76 ± 1.07	14.73 ± 0.84
30	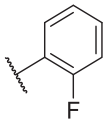	3.85 ± 0.63	3.96 ± 1.13	4.25 ± 0.49	4.85 ± 0.07	5.91 ± 0.28	6.95 ± 1.34
31	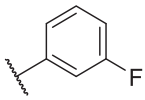	0.92 ± 0.11	1.81 ± 0.05	2.05 ± 0.42	2.76 ± 0.12	3.45 ± 0.21	5.46 ± 0.47
32	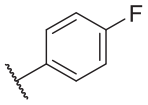	1.76 ± 0.37	2.12 ± 0.03	2.05 ± 0.42	3.75 ± 0.21	5.68 ± 0.14	6.93 ± 0.76
33	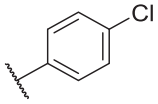	2.85 ± 0.21	3.06 ± 0.14	3.85 ± 0.35	7.65 ± 0.35	8.29 ± 0.28	9.95 ± 0.35
34	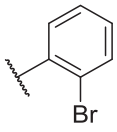	0.58 ± 0.08	1.16 ± 0.05	1.76 ± 0.53	1.98 ± 0.01	2.63 ± 0.15	3.63 ± 0.60
35	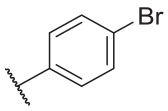	2.68 ± 0.28	3.78 ± 0.42	4.49 ± 0.14	8.65 ± 0.56	12.15 ± 0.07	18.25 ± 1.06
36	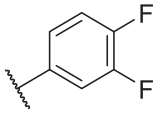	1.42 ± 0.14	1.36 ± 0.08	1.73 ± 0.17	1.73 ± 0.17	2.68 ± 0.03	2.56 ± 0.01
37	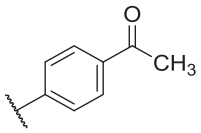	1.25 ± 0.07	2.03 ± 0.54	2.04 ± 0.12	2.61 ± 0.58	3.78 ± 0.10	5.01 ± 1.11
38	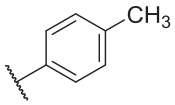	0.67 ± 0.17	1.22 ± 0.03	1.85 ± 0.28	2.51 ± 0.65	6.62 ± 0.49	10.17 ± 1.06
39	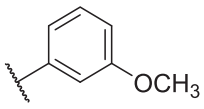	1.63 ± 0.22	1.87 ± 0.67	5.35 ± 0.07	14.17 ± 0.14	15.18 ± 1.50	16.35 ± 0.03

(*continued on next page*)

Table 2 (*continued*)

Cpd.	R	ARE–inducing activity in luciferase reporter assay (μM)[a,b]					
		0.01	0.1	1	20	40	80
40	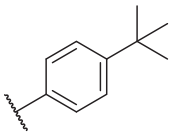	1.35 ± 0.67	2.88 ± 0.14	2.91 ± 0.44	8.35 ± 0.60	13.23 ± 0.83	24.02 ± 1.30
41	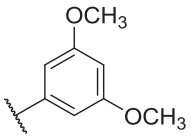	1.87 ± 0.28	1.91 ± 0.02	2.15 ± 0.91	3.45 ± 0.49	3.55 ± 0.07	4.45 ± 0.07
DMF		0.82 ± 0.04	1.00 ± 0.07	1.10 ± 0.08	1.65 ± 0.35	2.97 ± 0.45	ND
***t*BHQ**		1.18 ± 0.08	1.25 ± 0.01	1.24 ± 0.04	1.41 ± 0.07	2.14 ± 0.10	5.27 ± 0.41

[a] The inductivity of the compound was calculated compared to the blank control, and the data are presented as the mean ± SEM of three separate experiments.
[b] All compounds showed no significant anti-proliferative effects at the concentration of 80 μM.

Table 3
Physicochemical properties of the selected compounds.

Compound	Log*D*, pH 7.4	Intrinsic solubility, (μM)
1	3.37	66.90
6	3.30	99
24	2.86	200
25	3.07	250
26	2.65	220
29	4.75	16
35	3.91	77
38	4.16	35
39	3.91	86
40	3.92	91

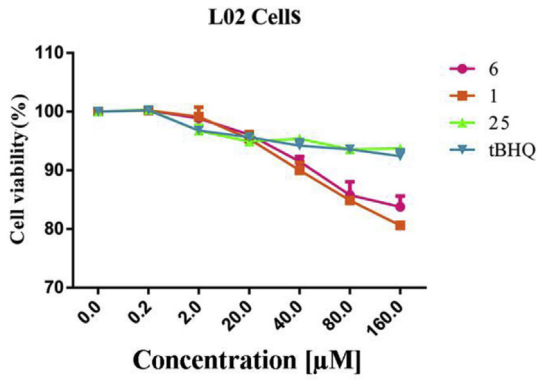

Fig. 2. Cytotoxicity evaluation of selected derivatives of ring A (**6**) and ring C (**25**) containing a 1,2,4-oxadiazole core in L02 cells. L02 cells were plated in a 96-well plate for 12 h and subsequently treated with different concentrations (0, 0.2, 2, 20, 40, 80, 160 μM) of the selected derivatives for another 24 h. Compound **1** and *t*BHQ were used as positive controls. The cell viability was measured by the MTT assay. All data represent the mean ± SD of three independent experiments.

the up-regulation of downstream antioxidant enzymes caused by **25** was based on Nrf2 activation. A subsequent qRT-PCR assay also confirmed the results that **25** could up-regulate the mRNA transcriptions of Nrf2, HO-1, NQO1, GCLC and GCLM in a concentration dependent manner (Fig. 3F). All these data indicated that **25** protected L02 cells through activating Nrf2-ARE antioxidant signaling pathway.

Induction of the transcription of antioxidant genes by activating the Nrf2-ARE cytoprotective pathway requires the transfer of Nrf2 from the cytoplasm to the nucleus. Therefore, we explored whether **25** could induce the accumulation of Nrf2 in the nucleus. An immunofluorescence assay confirmed that **25** induced Nrf2 accumulation in the nucleus of L02 cells. The green staining represents Nrf2, blue staining represents nucleus and the merge represents the nuclear import of Nrf2. The strong fluorescence in the nucleus indicated that Nrf2 translocated into the nucleus in a concentration-dependent manner compared to that in the control group (Fig. 4). The data further supported that **25** could induce Nrf2 translocation into the nucleus.

2.3.3. Protection of L02 cells from APAP-induced cytotoxicity by **25**

As a normal hepatic cell line, L02 cells are commonly used in hepatotoxicity studies induced by various hepatotoxic agents. It is well known that APAP overdose can cause liver damage. We selected three concentrations including 5, 10 and 20 μM, to evaluate the protective effects of **25** on APAP-induced hepatocyte injury. APAP (8 mM) was used to establish a cell damage model of L02 cells. L02 cells were plated in 96-well plates for 12 h and pretreated with **25** at different concentrations ranging from 5 μM to 20 μM for 24 h. The MTT cell proliferation assay showed that the L02 cells were damaged after APAP treatment for 24 h. We observed that **25** increased the proliferative capacity of (8 mM) APAP-challenged L02 cells in a concentration-dependent manner. Compound **25** at 20 μM increased the cell viability to approximately 80%, similar to *t*BHQ and DMF (Fig. 5). Additionally, to explore whether the liver protection of **25** was dependent on Nrf2 activation, we performed siRNA Nrf2 interference assays. The cell viability of L02 cells decreased to 50% when co-treated with siRNA Nrf2 and **25** (20 μM) compared to that in cells treated with **25** alone at the same concentration. All the results showed that **25** increased the cell viability in the hepatocyte injury model by Nrf2 activation.

2.3.4. Therapeutic effects of **25** on APAP-induced acute liver injury in a mouse model

To further investigate the potential protective effects of **25** on an APAP-induced acute liver injury mouse model, we measured the serum content of alanine aminotransferase (ALT) and aspartate aminotransferase (AST), which are regarded as common markers of liver damage. The contents of the model group increased remarkably compared to the normal group (Fig. 6A and B). Following treatment with different concentrations of **25** (10 mg/kg, 50 mg/kg and 100 mg/kg, respectively), the levels of ALT and AST were decreased in a concentration-dependent manner compared to those in the APAP model group. These results indicated that **25** exhibited potential therapeutic effects on APAP-induced acute liver

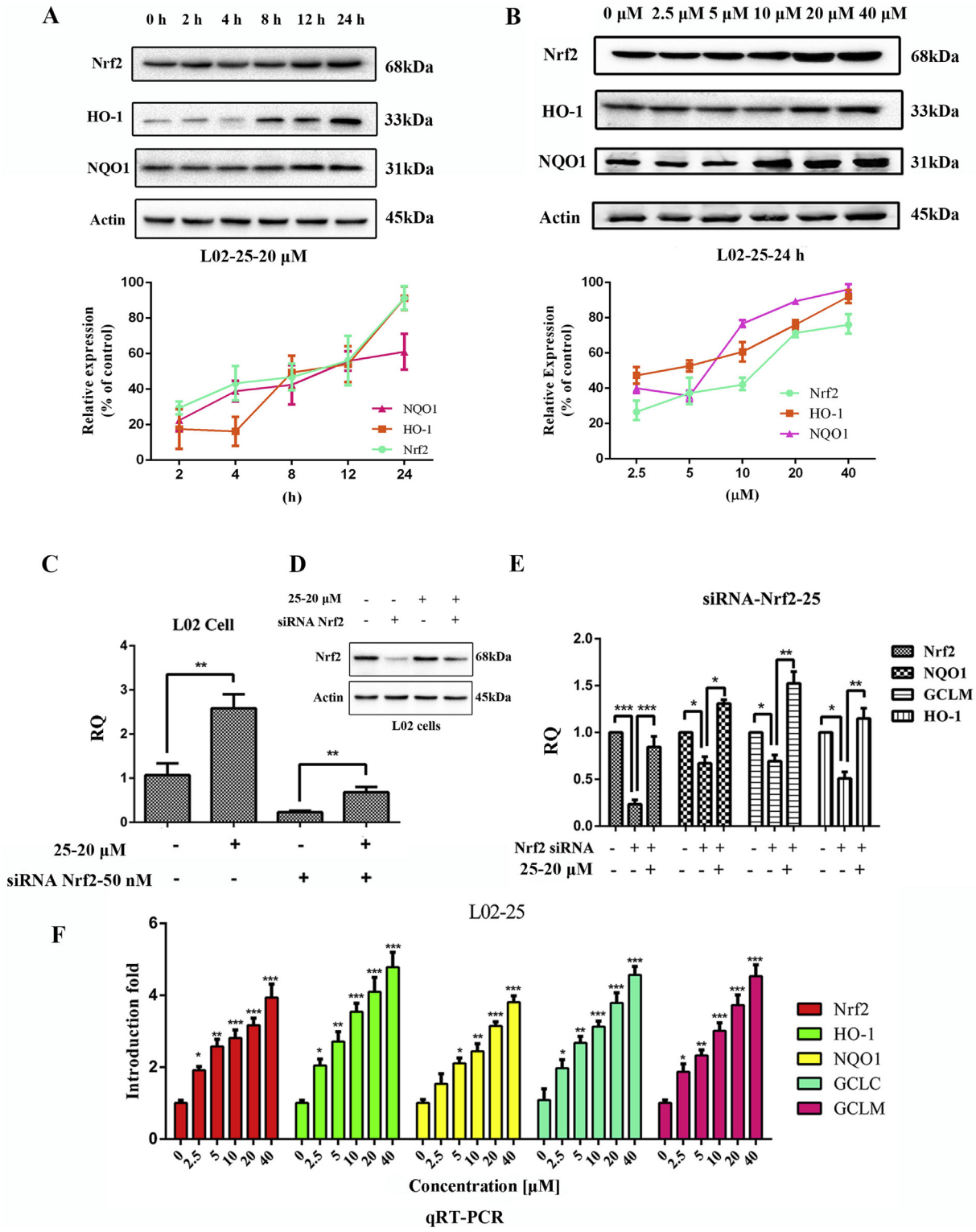

Fig. 3. (A) Time-dependent expression of Nrf2, HO-1 and NQO1 affected by **25**. After treatment with 20 μM **25** for 0, 2, 4, 8, 12, 24 h, cell lysates were prepared from L02 cells and subjected to western blot analysis. (B) Concentration-dependent expression of Nrf2, HO-1 and NQO1 affected by **25**. After treatment with **25** at different concentrations for 24 h, cell lysates were prepared from L02 cells and subjected to western blot analysis. Densitometric analysis was performed for each protein. All results were normalized to actin expression and are presented as the mean ± SD of three individual experiments. The data were analyzed using ImageJ 1.44p. (C) The mRNA transcription of Nrf2 after treatment with Nrf2 siRNA and **25**. L02 cells were treated with Nrf2 siRNA (50 nM), **25** (20 μM) or Nrf2 siRNA (50 nM) and **25** (20 μM). (D) Western blot analysis of Nrf2 protein after exposure to Nrf2 siRNA and **25** (20 μM). The L02 cells were treated with **25** (20 μM), Nrf2 siRNA (50 nM) or **25** (20 μM) plus Nrf2 siRNA (50 nM). Additional L02 cells were treated with DMSO for use as the blank control. (E) The mRNA transcription of Nrf2 and its downstream markers including NQO1, GCLM and HO-1 after treatment with Nrf2 siRNA and **25**. L02 cells were treated with Nrf2 siRNA (50 nM), **25** (20 μM) or Nrf2 siRNA (50 nM) and **25** (20 μM) separately. All genes transcription was determined by qRT-PCR. (F) Quantitative real-time PCR analysis of Nrf2, HO-1, NQO1, GCLC and GCLM in L02 cells. All genes transcription levels were determined after treatment with different concentrations (0, 2.5, 5, 10, 20, 40 μM) of **25** for 12 h. GAPDH was used as the control for normal expression of these genes. The values shown are the means ± SDs (n = 3). $^{*}p < 0.05$, $^{**}p < 0.01$, $^{***}p < 0.001$, statistically significant difference from the non-treated blank control group.

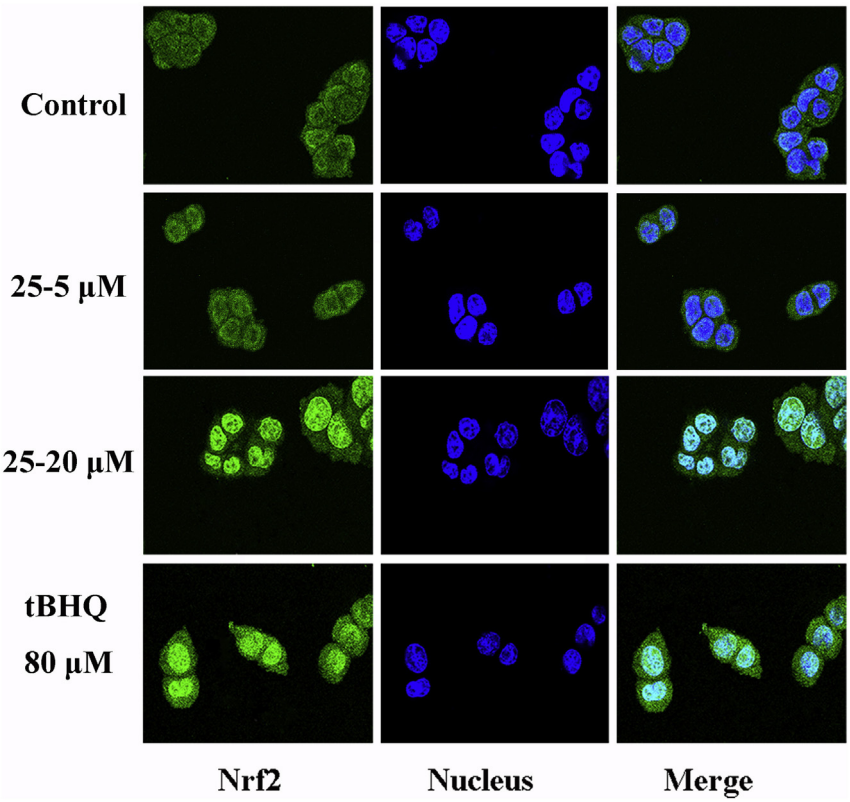

Fig. 4. Immunofluorescence staining of Nrf2 in L02 cells. Nrf2 and nuclei were labeled with DyLight 488 and DAPI, respectively. Green, Nrf2; blue, nuclei. Compound **25** (5 and 20 μM, respectively) was added and compared to the untreated control group. Cells treated with *t*BHQ (80 μM) served as the positive control (scale bar 20 μm). (For interpretation of the references to colour in this figure legend, the reader is referred to the Web version of this article.)

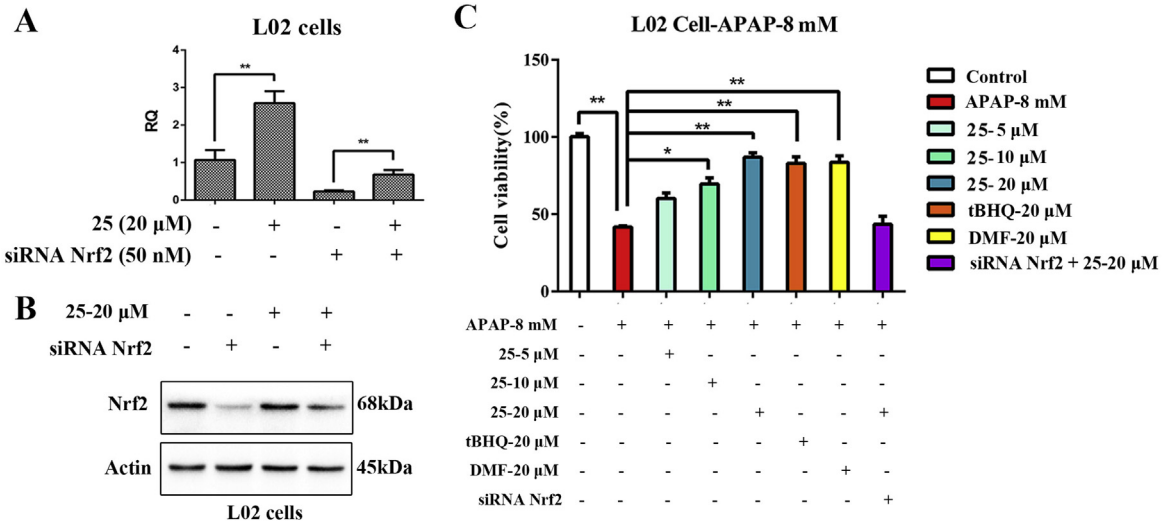

Fig. 5. Cytoprotection by **25** against damage induced by 8 mM APAP. (A) The mRNA transcription of Nrf2 after treatment of Nrf2 siRNA and **25**. The L02 cells were treated with Nrf2 siRNA (50 nM), **25** (20 μM) or Nrf2 siRNA (50 nM) and **25** (20 μM), respectively. (B) Western blot analysis of Nrf2 protein after exposure to Nrf2 siRNA and **25** (20 μM). The L02 cells were treated with **25** (20 μM), Nrf2 siRNA (50 nM) or **25** (20 μM) plus Nrf2 siRNA (50 nM). Additional L02 cells were treated with DMSO for use as the blank control. (C) L02 cells were plated in a 96-well plate for 12 h and subsequently treated with **25** at 5, 10 and 20 μM separately for another 24 h. An additional group was pre-treated with siRNA Nrf2 (50 nM) and evaluated after the administration of compound **25** at 20 μM. After the growth medium was replaced with medium containing APAP (8 mM) and incubation was continued for 24 h, the cell viability was measured by the MTT assay. *t*BHQ and DMF were used as positive controls. All data represent the mean ± SD of three independent experiments. $^{*}p < 0.05$, $^{**}p < 0.01$, statistically significant difference from the non-treated blank control group.

injury in mice and prevented APAP hepatotoxicity by reducing the expression of liver damage markers including ALT and AST in mouse serum.

Next, western blot and qRT-PCR analyses were used to confirm whether the liver protection by **25** was based on Nrf2-ARE pathway activation. The protein expression levels of Nrf2, HO-1 and NQO1 at

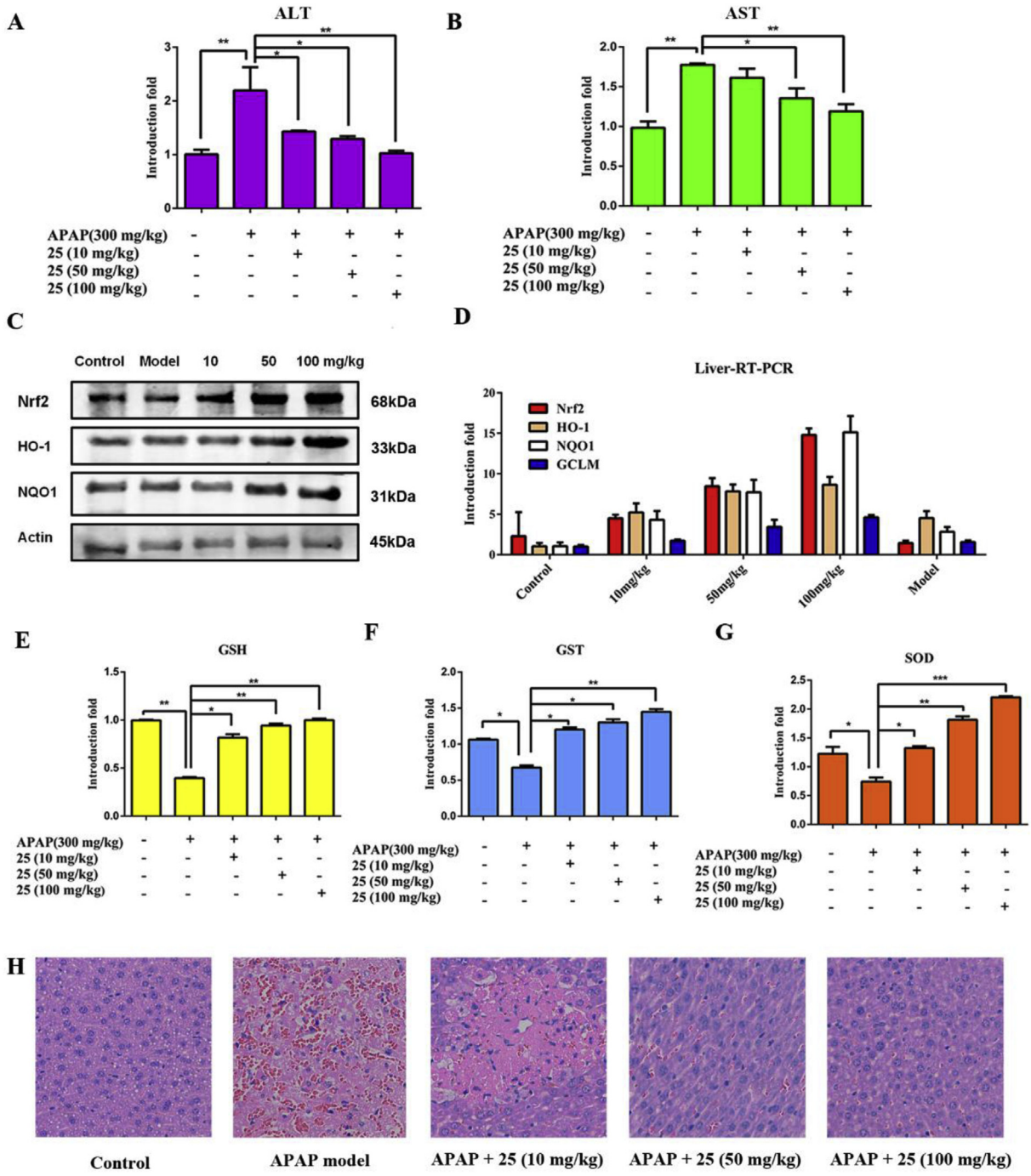

Fig. 6. (A&B) Protective effects of **25** on APAP-intoxicated mice. Mice received an intraperitoneal injection of **25** at 10 or 50 or 100 mg/kg (n = 10) once a day for seven days. The control group received the same volume of saline. After the seventh gavage of **25** or saline, the animals received a single injection of APAP (300 mg/kg). All mice were sacrificed at 24 h after APAP injection to obtain blood and liver samples. ALT (A) and AST (B) levels in mice serum. (C&D) Effects of **25** on the expression of Nrf2, HO-1 and NQO1 in APAP-intoxicated mice. The protein levels of Nrf2, HO-1 and NQO1 (C) were measured by western blot analysis as described in the materials and methods section. The protein expression levels were normalized to those of β-actin. The gene transcription levels of Nrf2, HO-1, NQO1 and GCLM (D) were measured by qRT-PCR analysis as described in the materials and methods section. The gene transcription levels were normalized to those of GAPDH. (E&F&G) Effects of **25** on the activities and protein expression of hepatic antioxidant enzymes in APAP-intoxicated mice. The contents of GSH (E), GST (F) and SOD (G) were measured as described in the materials and methods section. (H) Representative histological images of liver sections stained with hematoxylin and eosin (H&E) to evaluate the protective effects of **25**. The mice were intraperitoneally injected with **25** at 10, 50 or 100 mg/kg once a day for seven days. The control group received the same volume of saline. After the seventh gavage of **25** or saline, the animals received a single injection of APAP (300 mg/kg). All mice were sacrificed at 24 h after APAP injection to perform H&E staining. Typical images were chosen from each experimental group. The original magnification was 10 × 20. All data represent the means ± SD. Significant differences were presented as ***p< 0.001, **p < 0.01 or *p < 0.05 compared with the APAP group.

different concentrations of **25** were significantly higher than those in the model group (Fig. 6C). Subsequently, qRT-PCR was performed to examine the relative levels of Nrf2, HO-1, NQO1 and GCLM mRNA transcripts (Fig. 6D). Treatment with **25** (50 mg/kg and 100 mg/kg) elevated the relative levels of the Nrf2, HO-1, NQO1 and GCLM mRNA transcripts in a concentration-dependent manner. Thus, **25**

could activate the Nrf2-ARE pathway at both the protein and mRNA transcription levels, resulting in ideal therapeutic effects on the APAP-induced liver injury mouse model.

Additionally, the regulation of compound **25** on antioxidant enzymes (GSH, GST and SOD), which eliminate ROS and alleviate oxidative stress, was determined (Fig. 6E and F & G). The induction fold of antioxidases in the APAP-challenged model group was significantly decreased. Pretreatment with different concentrations of **25** (100 mg/kg, 50 mg/kg, 10 mg/kg) prior to APAP treatment significantly enhanced the release of GSH, GST and SOD in a concentration-dependent manner. As shown in Fig. 6H, histological analysis of liver tissue was performed using hematoxylin and eosin (H&E) staining. In the control group, the hepatocytes presented central rounded vesicular nucleus, while APAP triggered severe hepatocyte damage including massive cell necrosis (shown in APAP model group). Pretreatment of **25** reduced the APAP-induced liver damage in a concentration-dependent manner. Treatment with **25** significantly reduced the number of necrotic cells. The hepatic architecture following treatment with **25** at 100 mg/kg was approximately normal to that in the control group. Together, these results indicated that the therapeutic effects of **25** on APAP-induced acute liver injury in a mouse model were achieved by activating the Nrf2-ARE pathway. Compound **25** provides a promising therapeutic strategy to prevent APAP-induced liver injury.

3. Conclusion and discussion

Activating Nrf2 to resist environmental stress is generally believed to be a promising strategy [35]. Nrf2 up-regulates the transcriptions of several antioxidant and electrophile detoxifying genes via AREs present in their transcriptional promoters [36]. Activators of the Keap1-Nrf2-ARE pathway can induce the expression of phase II antioxidant enzymes, which further exert chemopreventive effects against a series of inflammation-related diseases including uncontrolled inflammation, cancer, neurodegenerative diseases, cardiovascular diseases and aging [37,38]. Therefore, discovering efficient activators of the Nrf2-ARE pathway is a promising approach and is urgently required.

We reported a series of novel Nrf2 activators with a 1,2,4-oxadiazole core and investigated the primary SAR of ring A. All analogues had three parts, including rings A, B and C. Among the derivatives, compound **1** (wherein *p*-fluorine was substituted in phenyl ring A) showed potent ARE-inducing activity [32]. Next, we investigated the changes in ARE-inducing activity when halogen substituents were introduced into phenyl ring A in various combinations. We synthesized sixteen compounds and evaluated their Nrf2-ARE inducing activities via the luciferase reporter gene assay. Among these compounds, **6** (*m*, *p*-F in ring A) showed more potent ARE-inducing activity than **1**. Based on compound **6** with the optimal ring A structure (*m*, *p*-F), we subsequently modified ring C and obtained twenty-five derivatives. Compound **25** (3′4-methylpyridineyl) at 80 μM exerted an optimal inducing activity that was 59.55-fold higher than that of **1** and **6** at the same concentration. The positions of the substituents on the phenyl or pyridine group did affect the Nrf2-ARE inducing activity. In contrast to ring A, electron-donating substituents in ring C promoted the Nrf2-ARE inducing activity, while electron-withdrawing substituents impaired this activity. Meanwhile, either no substituents or multiple substituents in ring C resulted in a decrease in ARE-inducing activity.

The protective effect of compound **25** on hepatocyte L02 cells and mouse liver tissues was studied in this paper. In addition, **25** exhibited a four-fold higher solubility compared to **1**. Despite the similar solubility of **24**, **25** and **26**, there were significant differences in ARE-inducing activities of them. This result may have been caused by differences in their spatial conformations.

Next, we performed further biological activity assessments and found that **25** could increase the transcription of Nrf2 downstream target genes including GCLM, NQO1 and HO-1. Compound **25** showed almost no cytotoxicity in normal liver cells (L02). Additionally, **25** could protect the liver against APAP-induced acute liver damage in mice via activating the Nrf2-ARE pathway. Compound **25** up-regulated antioxidant enzymes including GSH, GST and SOD and down-regulated the liver injury markers of AST and ALT in serum.

However, as a potent Nrf2 activator, **25** exhibits some indistinctive issues that need to be further validated. According to our experiment and research experience, we know that the absence of α, β-unsaturated carbonyl groups excludes the possibility of a Michael addition reaction activating the Nrf2-ARE pathway [39–41].

Above all, SAR studies on the 1,2,4-oxadiazole core provided guidance for subsequent structural modifications. The *in vivo* results regarding resistance to liver injury indicate that **25** is a promising novel hepato-protective agent that activates the Nrf2-ARE pathway. Compound **25** could be regarded as a potent Nrf2 activator for the treatment of APAP-induced liver injury.

4. Experimental section

4.1. General information

All reagents were purchased from commercial organizations. Organic solvent was concentrated in a rotary evaporator (Büchi Rotavapor) under reduced pressure below 55 °C degrees. Reactions were monitored by thin-layer chromatography (TLC) on 0.25 mm silica gel plates (GF254) and visualized under UV light. Melting points were measured with a Melt-Temp II apparatus. The ^{1}H NMR and ^{13}C NMR spectra were recorded on a Bruker AV-300 instrument using deuterated solvents with tetramethylsilane (TMS) as the internal standard. The purity (≥95%) of the compounds was verified by HPLC performed on an Agilent C_{18} (4.6 mm × 150 mm, 3.5 μm) column using a mixture of solvent methanol/water at a flow rate of 0.5 mL/min and peak detection at 254 nm under UV. ESI-mass spectra and high-resolution mass spectra (HRMS) were recorded on a Water Q-Tof micro mass spectrometer. IR spectra were determined on a Nicolet iS10 Avatar FT-IR spectrometer using KBr film.

4.2. Synthesis

4.2.1. Compounds ***1*–*16*** were synthesized using a similar method

4.2.1.1. 1H-benzo[d]imidazole-5-carbonitrile (***43***).

3,4-diaminobenzonitrile (**42**, 2.5 g; 18.75 mmol; 1.0 equiv) was dissolved in 5 M aqueous HCl (110 mL). The mixture was heated at 105 °C to reflux for 12 h. After stopping the reaction, the mixture was cooled to room temperature, basified with aqueous ammonia and stored overnight. The generated solid product was collected by filtration and washed with ice water. The products could be used without further purification. Yield: 2.5 g (94.0%). ^{1}H NMR (300 MHz, DMSO) δ 12.47 (s, 1H), 8.34 (s, 1H), 8.03 (s, 1H), 7.62 (d, J = 4.17 Hz, 1H), 7.45 (d, J = 8.34 Hz, 1H). MS *m/z*: 144.2 $[M + H]^{+}$.

4.2.1.2. (Z)-N′-Hydroxy-1H-benzo[d]imidazole-5-carboximidamide (***44***).

Compound **43** (2.5 g; 17.5 mmol; 1.0 equiv) was dissolved in EtOH (60 mL) treated with K_2CO_3 (4.32 g; 31.5 mmol; 1.8 equiv) and $H_2NOH{\cdot}HCl$ (2.25 g; 32.4 mmol; 1.8 equiv) and heated to reflux for 12 h. The mixture was diluted with diethyl ether when cooled to room temperature. The product was collected by filtration, washed with water, and dried under an infrared lamp. The compound was used without further purification. Yield: 1.54 g (50%). ^{1}H NMR

(300 MHz, DMSO) δ 13.10 (s, 1H), 10.86 (s, 1H), 8.50 (s, 1H), 8.32 (s, 2H), 8.03 (s, 1H), 7.74 (d, $J = 4.23$ Hz, 1H), 7.58 (d, $J = 4.23$ Hz, 1H). MS: 177.3 $[M+H]^+$.

*4.2.1.3. 3-(1H-Benzo[d]imidazol-6-yl)-5-(4-fluorophenyl)-1,2,4-oxadiazole (**1**).* 4-fluoro benzoic acid (0.16 g, 1.14 mmol, 1.0 equiv) was dissolved in DMF (3.0 mL) treated with carbonyldiimidazole (0.184 g, 1.14 mmol, 1.0 equiv) and stirred at room temperature for 1 h. Compound **44** (0.2 g, 1.14 mmol, 1.0 equiv) was added in the mixed solution and an additional 3 mL of DMF was added to the system. Next, the temperature was increased to 110 °C, and stirring was continued for 12–18 h. After cooling, the mixture was diluted using water and saturated aqueous $NaHCO_3$ solution. The generated solid product was collected by filtration and washed with saturated aqueous $NaHCO_3$ solution. Yield 26.2%. White solid; m. p. 186–187 °C. ^{1}H NMR (300 MHz, DMSO) δ 12.80 (s, 1H), 8.40 (s, 1H), 8.30–8.27 (m, 3H), 7.95 (d, $J = 8.22$ Hz, 1H), 7.78 (s, 1H), 7.55–7.49 (m, 2H). ^{13}C NMR (125 MHz, DMSO) δ 174.128, 168.867, 164.780 (d, $J = 251.13$ Hz), 143.950, 130.581 (d, $J = 9.25$ Hz), 120.731, 120.150, 119.626, 116.609 (d, $J = 22.34$ Hz), 115.861, 114.816. IR (cm^{-1}, KBr film): 3419 (−NH), 1620, 1095, 1023, 805. HRMS (ESI): calcd for $C_{15}H_{10}FN_4O$ $[M+H]^+$ 281.0833, found 281.0843. HPLC (80% methanol in water): $t_R = 7.43$ min, 98.88%.

*4.2.1.4. 3-(1H-benzo[d]imidazol-6-yl)-5-(4-chlorophenyl)-1,2,4-oxadiazol (**2**).* Yield 23.8%. White solid; m. p. 263–264 °C. ^{1}H NMR (300 MHz, DMSO) δ 12.79 (s, 1H), 8.51–8.48 (m, 2H), 8.22 (d, $J = 8.61$ Hz, 2H), 8.11–8.09 (m, 1H), 7.94–7.76 (m, 3H). ^{13}C NMR (75 MHz, DMSO) δ 175.075, 168.899, 145.221, 144.105, 133.199, 129.489, 129.489, 127.845, 127.845, 123.461, 120.853, 119.960, 118.335, 114.496, 112.632, 111.092. IR (cm^{-1}, KBr film): 3435 (−NH), 1611, 1106, 1021, 805. HRMS (ESI): calcd for $C_{15}H_{10}ClN_4O$ $[M+H]^+$ 297.0538, found 297.0535. HPLC (80% methanol in water): $t_R = 15.44$ min, 97.40%.

*4.2.1.5. 3-(1H-benzo[d]imidazol-6-yl)-5-(4-bromophenyl)-1,2,4-oxadiazol (**3**).* Yield 0.266 g (34.4%). White solid; m. p. 244–245 °C. ^{1}H NMR (300 MHz, DMSO) δ 12.79 (s, 1H), 8.40 (s, 1H), 8.33 (s, 1H), 8.16 (d, $J = 8.52$ Hz, 2H), 7.95 (d, $J = 8.82$ Hz, 1H), 7.90 (d, $J = 8.49$ Hz, 2H), 7.78 (d, $J = 8.04$ Hz, 1H). IR (cm^{-1}, KBr film): 3417 (−NH), 1611, 1098, 1029, 799. HRMS (ESI): calcd for $C_{15}H_{10}BrN_4O$ $[M+H]^+$ 341.0033, found 341.0023. HPLC (80% methanol in water): $t_R = 17.20$ min, 98.30%.

*4.2.1.6. 3-(1H-benzo[d]imidazol-6-yl)-5-(2-fluorophenyl)-1,2,4-oxadiazol (**4**).* Yield 38.9%. Brown solid; m. p. 233–236 °C. ^{1}H NMR (300 MHz, DMSO) δ 8.38 (s, 1H), 8.33 (s, 1H), 8.30–8.20 (m, 1H), 7.94 (d, $J = 7.27$ Hz, 1H), 7.86–7.73 (m, 2H), 7.62–7.44 (m, 2H). ^{13}C NMR (75 MHz, DMSO) δ 169.20, 162.11, 158.70, 144.86, 141.08, 139.09, 136.01, 135.90, 131.30, 125.91, 125.86, 121.16, 119.85, 117.84, 117.56, 116.56, 115.35. IR (cm^{-1}, KBr film): 3446 (−NH), 1622, 1400, 1091, 750. HRMS (ESI): calcd for $C_{15}H_{10}FN_4O$ $[M+H]^+$ 281.0833, found 281.0835. HPLC (80% methanol in water): $t_R = 6.01$ min, 95.11%.

*4.2.1.7. 3-(1H-benzo[d]imidazol-6-yl)-5-(3-fluorophenyl)-1,2,4-oxadiazol (**5**).* Yield 54%. White solid; m. p. 232–233 °C. ^{1}H NMR (300 MHz, DMSO) δ 12.79 (s, 1H), 8.40–8.33 (m, 2H), 8.10–7.90 (m, 3H), 7.82–7.66 (m, 2H), 7.66–7.55 (m, 1H). ^{13}C NMR (75 MHz, DMSO) δ 174.52, 174.48, 169.49, 164.27, 161.01, 144.56, 132.41, 132.30, 125.95, 125.84, 124.66, 124.62, 120.80, 120.52, 115.20, 114.88. IR (cm^{-1}, KBr film): 3447 (−NH), 1629, 1400, 1102, 754. HRMS (ESI): calcd for $C_{15}H_{10}FN_4O$ $[M+H]^+$ 281.0833, found 281.0839. HPLC (80% methanol in water): $t_R = 7.57$ min, 95.73%.

*4.2.1.8. 3-(1H-benzo[d]imidazol-6-yl)-5-(3,4-2fluorophenyl)-1,2,4-oxadiazol (**6**).* Yield 32%. White solid; m. p. 220–221 °C. ^{1}H NMR (300 MHz, DMSO) δ 12.79 (s, 1H), 8.39 (s, 1H), 8.30–8.19 (m, 2H), 8.19–8.04 (m, 1H), 8.02–7.90 (m, 1H), 7.82–7.66 (m, 2H). IR (cm^{-1}, KBr film): 3441 (−NH), 1623, 1400, 1101, 754. HRMS (ESI): calcd for $C_{15}H_9F_2N_4O$ $[M+H]^+$ 299.0739, found 299.0743. HPLC (80% methanol in water): $t_R = 8.67$ min, 97.53%.

*4.2.1.9. 3-(1H-benzo[d]imidazol-6-yl)-5-(2,3-2fluorophenyl)-1,2,4-oxadiazol (**7**).* Yield 33%. White solid; m. p. 219–220 °C. ^{1}H NMR (300 MHz, DMSO) δ 12.47 (s, 1H), 8.40 (s, 1H), 8.32 (s, 1H), 8.11–8.01 (m, 1H), 7.95 (dd, $J = 8.44$, 1.34 Hz, 1H), 7.90–7.74 (m, 2H), 7.57–7.43 (m, 1H). ^{13}C NMR (75 MHz, DMSO) δ 169.22, 159.98, 159.96, 158.41, 158.38, 156.78, 155.03, 155.01, 122.84, 122.72, 122.52, 122.40, 119.98, 119.87, 119.66, 119.55, 117.36, 117.34, 117.01, 116.99. IR (cm^{-1}, KBr film): 3448 (−NH), 1629, 1400, 1125, 989. HRMS (ESI): calcd for $C_{15}H_9F_2N_4O$ $[M+H]^+$ 299.0739, found 299.074. HPLC (80% methanol in water): $t_R = 9.29$ min, 97.86%.

*4.2.1.10. 3-(1H-benzo[d]imidazol-6-yl)-5-(2-chloro-4-fluorophenyl)-1,2,4-oxadiazol (**8**).* Yield 24.9%. White solid; m. p. 277–278 °C. ^{1}H NMR (300 MHz, DMSO) δ 12.80 (s, 1H), 8.55–8.22 (m, 3H), 8.01–7.80 (m, 3H), 7.56–7.50 (m, 1H), ^{13}C NMR (75 MHz, DMSO) δ 172.92, 168.64, 165.65, 162.27, 144.13, 134.25, 134.14, 134.12, 134.00, 119.65, 119.60, 119.02, 118.68, 115.74, 115.45. IR (cm^{-1}, KBr film): 3448 (−NH), 1637, 1400, 1089, 989. HRMS (ESI): calcd for $C_{15}H_9ClFN_4O$ $[M+H]^+$ 315.0443, found 315.0449. HPLC (80% methanol in water): $t_R = 8.62$ min, 96.11%.

*4.2.1.11. 3-(1H-benzo[d]imidazol-6-yl)-5-(3-chloro-4-fluorophenyl)-1,2,4-oxadiazol (**9**).* Yield 13%. White solid; m. p. 253–254 °C. ^{1}H NMR (300 MHz, DMSO) δ 7.93–7.76 (m, 5H), 7.57 (dd, $J = 5.6$, 2.0 Hz, 1H), 7.31 (dd, $J = 8.9$, 7.5 Hz, 1H). ^{13}C NMR (75 MHz, DMSO) δ 173.68, 162.11, 158.75, 144.62, 144.37, 138.68, 138.11, 130.69, 130.13, 129.73, 129.61, 129.47, 128.25, 121.80, 121.17, 120.25, 118.91, 118.62. IR (cm^{-1}, KBr film): 3448 (−NH), 1637, 1400, 1091, 988. HRMS (ESI): calcd for $C_{15}H_9ClFN_4O$ $[M+H]^+$ 315.0443, found 315.0449. HPLC (80% methanol in water): $t_R = 11.53$ min, 97.11%.

*4.2.1.12. 3-(1H-benzo[d]imidazol-6-yl)-5-(2,4-2fluorophenyl)-1,2,4-oxadiazol (**10**).* Yield 13%. White solid; m. p. 258–259 °C. ^{1}H NMR (300 MHz, DMSO) δ 12.78 (s, 1H), 8.39–8.26 (m, 3H), 7.93–7.41 (m, 3H), 7.39–7.36 (m, 1H). IR (cm^{-1}, KBr film): 3448 (−NH), 1623, 1400, 1090, 959. HRMS (ESI): calcd for $C_{15}H_9F_2N_4O$ $[M+H]^+$ 299.0739, found 299.0743. HPLC (80% methanol in water): $t_R = 6.68$ min, 98.22%.

*4.2.1.13. 3-(1H-benzo[d]imidazol-6-yl)-5-(3-chlorophenyl)-1,2,4-oxadiazol (**11**).* Yield 13.3%. White solid; m. p. 258–259 °C. ^{1}H NMR (300 MHz, DMSO) δ 8.51–8.32 (m, 2H), 8.18 (s, 2H), 8.04–7.79 (m, 4H). ^{13}C NMR (75 MHz, DMSO) δ 174.33, 169.46, 144.57, 134.59, 133.43, 131.96, 127.79, 127.00, 125.81, 121.28, 119.95, 116.45, 116.37, 115.40, 115.36. IR (cm^{-1}, KBr film): 3447 (−NH), 1629, 1400, 1092, 987. HRMS (ESI): calcd for $C_{15}H_{10}ClN_4O$ $[M+H]^+$ 297.0538, found 297.0546. HPLC (80% methanol in water): $t_R = 10.57$ min, 98.23%.

*4.2.1.14. 3-(1H-benzo[d]imidazol-6-yl)-5-(2,5-2fluorophenyl)-1,2,4-oxadiazol (**12**).* Yield 47.6%. White solid; m. p. 261–262 °C. ^{1}H NMR (300 MHz, DMSO) δ 12.79 (s, 1H), 8.39–8.32 (m, 2H), 8.06–7.78 (m, 2H), 7.72–7.58 (m, 3H). ^{13}C NMR (75 MHz, DMSO) δ 169.17, 159.94, 159.91, 158.36, 158.33, 156.73, 156.69, 154.99, 154.96, 144.55, 122.77, 122.65, 122.45, 122.33, 121.27, 119.91, 119.80, 119.60, 119.48, 117.26, 117.25, 116.91, 116.89, 113.58, 113.46, 113.39, 113.27. IR (cm^{-1}, KBr film): 3448 (−NH), 1629, 1400, 1088, 990. HRMS (ESI): calcd for $C_{15}H_9F_2N_4O$ $[M+H]^+$ 299.0739, found 299.0743. HPLC (80%

methanol in water): $t_R = 6.64$ min, 96.08%.

*4.2.1.15. 3-(1H-benzo[d]imidazol-6-yl)-5-(2-bromo-4-fluorophenyl)-1,2,4-oxadiazol (**13**).* Yield 32.9%. White solid; m. p. 233–234 °C. ^{1}H NMR (300 MHz, DMSO) δ 12.80 (s, 1H), 8.55–8.19 (m, 3H), 8.10–7.96 (m, 2H), 7.94–7.76 (m, 2H), 7.58–7.18 (m, 1H). ^{13}C NMR (75 MHz, DMSO) δ 169.14, 165.87, 162.47, 144.66, 134.89, 134.76, 134.04, 131.03, 125.45, 122.53, 122.20, 119.66, 118.26, 116.50, 116.21. IR (cm^{-1}, KBr film): 3446 (–NH), 1628, 1400, 1091, 988. HRMS (ESI): calcd for $C_{15}H_9BrFN_4O$ $[M + H]^+$ 358.9938, found 358.9946. HPLC (80% methanol in water): $t_R = 8.73$ min, 95.34%.

*4.2.1.16. 3-(1H-benzo[d]imidazol-6-yl)-5-(3-bromo-4-fluorophenyl)-1,2,4-oxadiazol (**14**).* Yield 5.4%. White solid; m. p. 268–269 °C. ^{1}H NMR (300 MHz, DMSO) δ 12.81 (s, 1H), 8.58 (s, 1H), 8.41–8.32 (m, 1H), 8.30–8.29 (m, 1H), 8.02 (s, 1H), 7.97–7.78 (m, 1H), 7.56 (s, 1H), 7.16 (s, 1H). ^{13}C NMR (75 MHz, DMSO) δ 169.15, 165.86, 162.48, 144.61, 134.89, 134.76, 134.04, 131.04, 125.45, 122.53, 122.20, 119.65, 118.25, 116.50, 116.21. IR (cm^{-1}, KBr film): 3448 (–NH), 1637, 1400, 1074, 988. HRMS (ESI): calcd for $C_{15}H_9BrFN_4O$ $[M + H]^+$ 358.9938, found 358.9942. HPLC (80% methanol in water): $t_R = 5.82$ min, 98.86%.

*4.2.1.17. 3-(1H-benzo[d]imidazol-6-yl)-5-(2,4,5-3fluorophenyl)-1,2,4-oxadiazol (**15**).* Yield 7%. White solid; m. p. 216–217 °C. ^{1}H NMR (300 MHz, DMSO) δ 8.36–8.26 (m, 2H), 8.13–8.07 (m, 1H), 7.94–7.77 (m, 1H), 7.75 (s, 1H), 7.20 (s, 1H). ^{13}C NMR (75 MHz, DMSO) δ 169.68, 158.28, 158.23, 154.95, 154.89, 144.65, 138.71, 138.37, 137.63, 130.02, 129.91, 129.68, 121.36, 121.18, 120.31, 113.03, 112.79, 112.70, 112.68. IR (cm^{-1}, KBr film): 3448 (–NH), 1638, 1400, 1092, 988. HRMS (ESI): calcd for $C_{15}H_8F_3N_4O$ $[M + H]^+$ 317.0645, found 317.0644. HPLC (80% methanol in water): $t_R = 4.91$ min, 95.46%.

*4.2.1.18. 3-(1H-benzo[d]imidazol-6-yl)-5-(2,4-2fluoro-5-chlorophenyl)-1,2,4-oxadiazol (**16**).* Yield 10.3%. White solid; m. p. 217–218 °C. ^{1}H NMR (300 MHz, DMSO) δ 12.80 (s, 1H), 8.57 (s, 1H), 8.38 (s, 1H), 8.16 (s, 1H), 8.01–7.69 (m, 1H), 7.50 (s, 1H). IR (cm^{-1}, KBr film): 3449 (–NH), 1637, 1400, 1090, 987. ^{13}C NMR (75 MHz, DMSO) δ 169.26, 158.26, 154.88, 151.78, 137.83, 137.75, 130.32, 120.12, 120.07, 119.11, 118.77, 118.75, 114.16, 113.80. HRMS (ESI): calcd for $C_{15}H_8ClF_2N_4O$ $[M + H]^+$ 332.0645, found 332.0644. HPLC (80% methanol in water): $t_R = 4.92$ min, 95.53%.

*4.2.2. Intermediates **45~76** were synthesized using a similar method*

*4.2.2.1. (Z)-N′-Hydroxy-pyridine-2-carboxamidine (**45**).* 2-cyanopyridine (2.5 g, 24.01 mmol) was dissolved in EtOH (60 mL) treated with K_2CO_3 (5.97 g; 43.22 mmol; 1.8 equiv) and $H_2NOH \cdot HCl$ (3.0 g; 43.22 mmol; 1.8 equiv) and heated to reflux for 12 h. The mixture was diluted with diethyl ether when it was cooled to room temperature. The product was collected by filtration, washed with water, and dried under an infrared lamp. The compound was used without further purification. Yield: 1.5 g (45.5%). m. p. 184–185 °C. ^{1}H NMR (300 MHz, DMSO) δ 9.93 (s, 1H), 8.56–8.54 (m, 1H), 7.87–7.77 (m, 2H), 7.42–7.37 (m, 1H), 5.84 (s, 2H). EI-MS *m/z*: 136.1 $[M]^+$. HPLC (80% methanol in water): $t_R = 6.57$ min, 97.68%.

*4.2.2.2. (Z)-N′-Hydroxy-pyridine-4-carboxamidine (**46**).* Yield: 1.3 g (39.5%). m. p. 185–186 °C. ^{1}H NMR (300 MHz, DMSO) δ 10.06 (s, 1H), 8.58–8.55 (m, 2H), 7.65–7.62 (m, 2H), 6.03 (s, 2H). EI-MS *m/z*: 136.1 $[M]^+$. HPLC (80% methanol in water): $t_R = 5.57$ min, 96.78%.

*4.2.2.3. (Z)-N′-Hydroxy-pyridine-3-carboxamidine (**47**).* Yield: 1.6 g (48.6%). m. p. 187–188 °C. ^{1}H NMR (300 MHz, DMSO) δ 9.85 (s, 1H), 8.85 (s, 1H), 8.55 (d, $J = 3.45$ Hz, 1H), 8.01 (d, $J = 7.41$ Hz, 1H), 7.42–7.37 (m, 1H), 6.00 (s, 2H). EI-MS *m/z*: 136.1 $[M]^+$. HPLC (80% methanol in water): $t_R = 4.87$ min, 95.38%.

*4.2.2.4. (Z)-N′-Hydroxy-5-fluoropyridine-2-carboxamidine (**48**).* Yield: 1.2 g (37.7%). m. p. 186–187 °C. ^{1}H NMR (300 MHz, DMSO) δ 9.96 (s, 1H), 8.55 (d, $J = 2.88$ Hz, 1H), 7.93–7.88 (m, 1H), 7.78–7.71 (m, 1H), 5.85 (s, 2H). EI-MS *m/z*: 154.1 $[M]^+$. HPLC (80% methanol in water): $t_R = 7.57$ min, 98.58%.

*4.2.2.5. (Z)-N′-Hydroxy-6-methylpyridine-2-carboxamidine (**49**).* Yield: 1.7 g (53%). m. p. 179–180 °C. ^{1}H NMR (300 MHz, DMSO) δ 9.74 (s, 1H), 8.71 (d, $J = 1.65$ Hz, 1H), 7.89 (dd, $J = 2.10$, 8.07 Hz, 1H), 7.24 (d, $J = 8.10$ Hz, 1H), 5.93 (s, 2H), 2.46 (s, 3H). EI-MS *m/z*: 150.1 $[M]^+$. HPLC (80% methanol in water): $t_R = 5.87$ min, 97.61%.

*4.2.2.6. (Z)-N′-Hydroxy-pyrazine-2-carboxamidine (**50**).* Yield: 1.4 g (42.6%). m. p. 219–220 °C. ^{1}H NMR (300 MHz, DMSO) δ 10.19 (s, 1H), 8.83 (d, $J = 4.86$ Hz, 2H), 7.49 (t, $J = 4.86$ Hz, 1H), 5.84 (s, 2H). EI-MS *m/z*: 137.1$[M]^+$. HPLC (80% methanol in water): $t_R = 7.15$ min, 98.53%.

*4.2.2.7. (Z)-N′-Hydroxy-pyrimidine-2-carboxamidine (**51**).* Yield: 1.5 g (45.7%). m. p. 211–212 °C. ^{1}H NMR (300 MHz, DMSO) δ 10.19 (s, 1H), 8.83 (d, $J = 4.86$ Hz, 2H), 7.51 (t, $J = 4.86$ Hz, 1H), 5.84 (s, 2H). EI-MS *m/z*: 137.1$[M]^+$. HPLC (80% methanol in water): $t_R = 8.34$ min, 99.25%.

*4.2.2.8. (Z)-N′-Hydroxy-1H-indole-4-carboxamidine (**52**).* Yield: 1.1 g (35.7%). m. p. 189–190 °C. ^{1}H NMR (300 MHz, DMSO) δ 11.19 (s, 1H), 9.57 (s, 1H), 7.42–7.23 (m, 3H), 7.11–7.05 (m, 1H), 6.82 (d, $J = 2.49$ Hz, 1H), 5.68 (s, 2H). EI-MS *m/z*: 174.1$[M]^+$. HPLC (80% methanol in water): $t_R = 7.51$ min, 96.65%.

*4.2.2.9. (Z)-N′-Hydroxy-naphthalene-2-carboxamidine (**53**).* Yield: 1.3 g (42.7%). m. p. 206–207 °C. ^{1}H NMR (300 MHz, DMSO) δ 8.01–7.85 (m, 3H), 7.80 (s, 1H), 7.77–7.68 (m, 2H), 7.69–7.48 (m, 5H), 4.59 (s, 2H), 3.87 (d, $J = 13.80$ Hz, 1H), 3.38 (d, $J = 13.80$ Hz, 1H). EI-MS *m/z*: 185.1$[M]^+$. HPLC (80% methanol in water): $t_R = 5.34$ min, 95.64%.

*4.2.2.10. (Z)-N′-hydroxy-[1,1′-biphenyl]-4-carboximidamide (**54**).* Yield: 1.0 g (33.7%). m. p. 146–147 °C. ^{1}H NMR (300 MHz, DMSO) δ 9.69 (s, 1H), 7.78–7.65 (m, 6H), 7.49–7.34 (m, 3H), 5.86 (s, 2H). EI-MS *m/z*: 211.1$[M]^+$. HPLC (80% methanol in water): $t_R = 9.53$ min, 96.53%.

*4.2.2.11. (Z)-N′-hydroxy-4-methylbenzimidamide (**55**).* Yield: 1.4 g (43.7%). m. p. 193–194 °C. ^{1}H NMR (300 MHz, DMSO) δ 9.55 (s, 1H), 7.55 (d, $J = 8.16$ Hz, 2H), 7.16 (d, $J = 7.98$ Hz, 2H), 5.75 (s, 2H), 2.30 (s, 3H). EI-MS *m/z*: 149.1$[M]^+$. HPLC (80% methanol in water): $t_R = 7.54$ min, 97.86%.

*4.2.2.12. (Z)-4-Acetyl-N′-hydroxybenzimidamide (**56**).* Yield: 1.5 g (48%). m. p. 194–195 °C. ^{1}H NMR (300 MHz, DMSO) δ 7.85 (d, $J = 7.51$ Hz, 2H), 7.38 (d, $J = 7.51$ Hz, 2H), 4.59 (s, 2H), 3.83 (d, $J = 13.80$ Hz, 1H), 3.37 (d, $J = 13.80$ Hz, 1H), 2.51 (s, 3H). EI-MS *m/z*: 177.1$[M]^+$. HPLC (80% methanol in water): $t_R = 6.75$ min, 96.45%.

*4.2.2.13. (Z)-2-Fluoro-N′-hydroxybenzimidamide (**57**).* Yield: 1.6 g (50.3%). m. p. 146–147 °C. ^{1}H NMR (300 MHz, DMSO) δ 9.68 (s, 1H), 7.52–7.38 (m, 2H), 7.29–7.17 (m, 2H), 5.81 (s, 2H). EI-MS *m/z*: 153.1 $[M]^+$. HPLC (80% methanol in water): $t_R = 5.65$ min, 98.85%.

*4.2.2.14. (Z)-3-Fluoro-N′-hydroxybenzimidamide (**58**).* Yield: 1.4 g

(44%). m. p. 180–181 °C. ^{1}H NMR (300 MHz, DMSO) δ 9.79 (s, 1H), 7.65–7.37 (m, 3H), 7.26–7.16 (m, 1H), 5.90 (s, 2H). EI-MS *m/z*: 153.1 $[M]^+$. HPLC (80% methanol in water): $t_R = 6.34$ min, 97.85%.

*4.2.2.15. (Z)-4-Fluoro-N′-hydroxybenzimidamide (**59**).* Yield: 1.43 g (45%). m. p. 222–223 °C. ^{1}H NMR (300 MHz, DMSO) δ 9.65 (s, 1H), 7.73–7.68 (m, 2H), 7.25–7.16 (m, 2H), 5.85 (s, 2H). EI-MS *m/z*: 153.1 $[M]^+$. HPLC (80% methanol in water): $t_R = 7.27$ min, 98.73%.

*4.2.2.16. (Z)-3-Methoxy-N′-hydroxybenzimidamide (**60**).* Yield: 1.6 g (51%). m. p. 205–206 °C. ^{1}H NMR (300 MHz, DMSO) δ 9.63 (s, 1H), 7.30–7.21 (m, 3H), 6.95–6.91 (m, 1H), 5.81 (s, 2H), 3.76 (s, 3H). EI-MS *m/z*: 165.1$[M]^+$. HPLC (80% methanol in water): $t_R = 6.64$ min, 99.10%.

*4.2.2.17. (Z)-3,4-Difluoro-N′-hydroxybenzimidamide (**61**).* Yield: 1.0 g (32%). m. p. 189–190 °C. ^{1}H NMR (300 MHz, DMSO) δ 9.77 (s, 1H), 7.87–7.39 (m, 3H), 5.94 (s, 2H). EI-MS *m/z*: 171.1$[M]^+$. HPLC (80% methanol in water): $t_R = 8.56$ min, 95.74%.

*4.2.2.18. (Z)-4-Chloro-N′-hydroxybenzimidamide (**62**).* Yield: 1.1 g (35.4%). m. p. 184–185 °C. ^{1}H NMR (300 MHz, DMSO) δ 7.37 (d, $J = 7.53$ Hz, 2H), 7.22 (d, $J = 7.53$ Hz, 2H), 4.59 (s, 2H), 3.79 (d, $J = 13.80$ Hz, 1H), 3.34 (d, $J = 13.80$ Hz, 1H). EI-MS *m/z*: 169.1$[M]^+$. HPLC (80% methanol in water): $t_R = 6.89$ min, 97.63%.

*4.2.2.19. (Z)-2-Bromo-N′-hydroxybenzimidamide (**63**).* Yield: 1.2 g (41%). m. p. 191–192 °C. ^{1}H NMR (300 MHz, DMSO) δ 7.87 (s, 1H), 7.71–7.56 (m, 2H), 7.39–7.17 (m, 3H). EI-MS *m/z*: 214.1$[M]^+$. HPLC (80% methanol in water): $t_R = 7.63$ min, 97.71%.

*4.2.2.20. (Z)-4-(tert-butyl)-N′-hydroxybenzimidamide (**64**).* Yield: 1.1 g (36.4%). m. p. 177–178 °C. ^{1}H NMR (300 MHz, DMSO) δ 9.56 (s, 1H), 7.59 (d, $J = 8.40$ Hz, 2H), 7.37 (d, $J = 8.43$ Hz, 2H), 5.75 (s, 2H), 1.28 (s, 9H). EI-MS *m/z*: 191.1$[M]^+$. HPLC (80% methanol in water): $t_R = 7.85$ min, 96.43%.

*4.2.2.21. (Z)-N′-Hydroxy-6-methylpyridine-3-carboxamidine (**65**).* Yield: 1.4 g (40%). m. p. 172–173 °C. ^{1}H NMR (300 MHz, DMSO) δ 9.74 (s, 1H), 8.71 (d, $J = 1.65$ Hz, 1H), 7.89 (dd, $J = 2.10$, 8.07 Hz, 1H), 7.24 (d, $J = 8.10$ Hz, 1H), 5.93 (s, 2H), 2.46 (s, 3H). EI-MS *m/z*: 150.1 $[M]^+$. HPLC (80% methanol in water): $t_R = 8.67$ min, 98.63%.

*4.2.2.22. (Z)-N′-Hydroxy-4-methylpyridine-2-carboxamidine (**66**).* Yield: 1.0 g (31%). m. p. 167–168 °C. ^{1}H NMR (300 MHz, DMSO) δ 9.86 (s, 1H), 8.40 (d, $J = 4.95$ Hz, 1H), 7.67 (s, 1H), 7.22 (d, $J = 4.95$ Hz, 1H), 5.81 (s, 2H), 2.33 (s, 3H). EI-MS *m/z*: 150.1$[M]^+$. HPLC (80% methanol in water): $t_R = 8.14$ min, 99.75%.

*4.2.2.23. (Z)-N′-Hydroxy-3-fluoropyridine-2-carboxamidine (**67**).* Yield: 1.3 g (41%). m. p. 179–180 °C. ^{1}H NMR (300 MHz, DMSO) δ 10.13 (s, 1H), 8.46–8.44 (m, 1H), 7.53–7.47 (m, 1H), 5.85 (s, 2H). EI-MS *m/z*: 154.1$[M]^+$. HPLC (80% methanol in water): $t_R = 8.62$ min, 99.43%.

*4.2.2.24. (Z)-3,5-Dimethoxy-N′-hydroxybenzimidamide (**68**).* Yield: 1.4 g (46.7%). m. p. 209–210 °C. ^{1}H NMR (300 MHz, DMSO) δ 9.63 (s, 1H), 6.84 (d, $J = 2.04$ Hz, 1H), 6.49 (t, $J = 1.98$ Hz, 1H), 5.80 (s, 2H), 3.74 (s, 6H). EI-MS *m/z*: 195.1$[M]^+$. HPLC (80% methanol in water): $t_R = 9.61$ min, 98.71%.

*4.2.2.25. (Z)-4-Bromo-N′-hydroxybenzimidamide (**69**).* Yield: 1.2 g (41%). m. p. 174–175 °C. ^{1}H NMR (300 MHz, DMSO) δ 9.76 (s, 1H), 7.64–7.54 (m, 4H), 5.88 (s, 2H). EI-MS *m/z*: 214.0$[M]^+$. HPLC (80% methanol in water): $t_R = 7.92$ min, 99.17%.

*4.2.3. Compound **17**–**41** were synthesized using a similar method*

*4.2.3.1. 5-(3,4-difluorophenyl)-3-(pyridin-2-yl)-1,2,4-oxadiazole (**17**).* 3,4-difluorobenzoic acid (0.46 g, 2.92 mmol, 1.0 equiv) was dissolved in DMF (3.0 mL) treated with carbonyldiimidazole (0.48 g, 2.92 mmol, 1.0 equiv) and stirred at room temperature for 1 h. **45** (0.4 g, 2.92 mmol, 1.0 equiv) was added in the mixed solution and another 3 mL DMF was added in the system. Then the temperature was increased to 110 °C and stirring was continued for 12–18 h. After cooling, the mixture was diluted by means of water and saturated aqueous $NaHCO_3$ solution. The generated solid product was collected by filtration and washed with saturated aqueous $NaHCO_3$ solution. Yield: 0.345 g (45.6%). White solid; m. p. 144–145 °C. ^{1}H NMR (300 MHz, DMSO) δ 8.80 (s, 1H), 8.18–8.04 (m, 2H), 7.98–7.96 (m, 2H), 7.90–7.64 (m, 2H). ^{13}C NMR (75 MHz, DMSO) δ 173.688, 168.412, 164.187, 161.069, 150.291, 145.234, 137.666, 126.260, 126.050, 123.403, 111.596, 111.221, 108.896. HRMS (ESI): calcd for $C_{13}H_7F_2N_3ONa$ $[M + Na]^+$ 282.04494, found 282.04609. HPLC (80% methanol in water): $t_R = 9.82$ min, 96.93%.

*4.2.3.2. 5-(3,4-difluorophenyl)-3-(pyridin-4-yl)-1,2,4-oxadiazole (**18**).* Yield: 0.304 g (40.2%). White solid; m. p. 168–169 °C. ^{1}H NMR (300 MHz, DMSO) δ 8.87 (s, 2H), 8.03–7.92 (m, 4H), 7.81–7.67 (m, 1H). ^{13}C NMR (75 MHz, DMSO) δ 175.59, 168.55, 165.81, 165.64, 162.51, 162.35, 152.34, 134.44, 127.30, 122.38, 113.18, 113.06, 112.93, 112.81, 110.89, 110.55, 110.20. HRMS (ESI): calcd for $C_{13}H_8F_2N_3O$ $[M + H]^+$ 260.06299, found 260.06408. HPLC (80% methanol in water): $t_R = 8.34$ min, 99.25%.

*4.2.3.3. 5-(3,4-difluorophenyl)-3-(pyridin-3-yl)-1,2,4-oxadiazole (**19**).* Yield: 0.295 g (39.2%). White solid; m. p. 123–124 °C. ^{1}H NMR (300 MHz, DMSO) δ 9.24–9.21 (m, 1H), 8.82–8.77 (m, 1H), 8.55–8.07 (m, 3H), 7.75–7.41 (m, 2H). ^{13}C NMR (75 MHz, DMSO) δ 167.37, 167.18, 163.83, 151.27, 151.14, 133.77, 131.41, 131.28, 130.25, 129.80, 121.41, 121.02, 117.47, 117.17, 112.00. HRMS (ESI): calcd for $C_{13}H_8F_2N_3O$ $[M + H]^+$ 260.06299, found 260.06581. HPLC (80% methanol in water): $t_R = 9.63$min, 97.43%.

*4.2.3.4. 5-(3,4-difluorophenyl)-3-(5-fluoropyridin-2-yl)-1,2,4-oxadiazole (**20**).* Yield: 0.315 g (44.3%). White solid; m. p. 162–163 °C. ^{1}H NMR (300 MHz, DMSO) δ 8.84 (s, 1H), 8.29–7.25 (m, 1H), 8.06–7.91 (m, 3H), 7.79–7.72 (m, 1H). ^{13}C NMR (75 MHz, DMSO) δ 169.02, 165.79, 165.62, 163.26, 162.50, 162.33, 159.83, 143.17, 140.50, 140.17, 126.75, 126.68, 126.06, 125.81, 113.05, 112.93, 112.81, 112.68, 110.71, 110.37, 110.03. HRMS (ESI): calcd for $C_{13}H_7F_3N_3O$ $[M + H]^+$ 278.05357, found 278.05565. HPLC (80% methanol in water): $t_R = 10.51$ min, 97.51%.

*4.2.3.5. 5-(3,4-difluorophenyl)-3-(3-fluoropyridin-2-yl)-1,2,4-oxadiazole (**21**).* Yield: 0.345 g (48.5%). White solid; m. p. 146–147 °C. ^{1}H NMR (300 MHz, DMSO) δ 8.67 (d, $J = 2.85$ Hz, 1H), 8.06–7.99 (m, 1H), 7.89–7.87 (m, 2H), 7.80–7.67 (m, 2H). ^{13}C NMR (75 MHz, DMSO) δ 165.79, 165.62, 162.49, 162.32, 161.08, 147.73, 147.66, 129.66, 129.60, 127.01, 126.77, 113.05, 112.92, 112.81, 112.68, 110.72, 110.37, 110.03. HRMS (ESI): calcd for $C_{13}H_6F_3N_3ONa$ $[M + Na]^+$ 300.03552, found 300.03671. HPLC (80% methanol in water): $t_R = 10.71$ min, 98.81%.

*4.2.3.6. 5-(3,4-difluorophenyl)-3-(pyrazin-2-yl)-1,2,4-oxadiazole (**22**).* Yield: 0.345 g (46.0%). White solid; m. p. 217–218 °C. ^{1}H NMR (300 MHz, DMSO) δ 9.38 (s, 1H), 8.92 (s, 2H), 8.22–8.18 (m, 1H), 7.74 (s, 1H), 7.20 (s, 1H). ^{13}C NMR (75 MHz, DMSO) δ 156.00, 147.74, 145.72, 144.42, 141.86, 137.77, 130.20, 126.73, 125.89, 125.85, 120.28, 117.52, 117.21. HRMS (ESI): calcd for $C_{12}H_7F_2N_4O$ $[M + H]^+$ 261.05824, found 261.05841. HPLC (80% methanol in water): $t_R = 9.63$ min, 97.68%.

*4.2.3.7. 5-(3,4-difluorophenyl)-3-(pyrimidin-2-yl)-1,2,4-oxadiazole (**23**).* Yield: 0.295 g (39.3%). White solid; m. p. 202–203 °C. ^{1}H NMR (300 MHz, DMSO) δ 9.09 (d, *J* = 4.89 Hz, 2H), 7.93 (d, *J* = 5.55 Hz, 2H), 7.82–7.67 (m, 2H). ^{13}C NMR (75 MHz, DMSO) δ 175.53, 168.53, 165.80, 165.63, 162.50, 162.33, 159.64, 156.37, 127.76, 124.42, 113.06, 112.94, 112.82, 112.69, 110.73, 110.39, 110.05. HRMS (ESI): calcd for $C_{12}H_7F_2N_4O$ [M + H]$^+$ 261.05824, found 261.05841. HPLC (80% methanol in water): t_R = 9.89 min, 98.74%.

*4.2.3.8. 5-(3,4-difluorophenyl)-3-(6-methylpyridin-2-yl)-1,2,4-oxadiazole (**24**).* Yield: 0.285 g (39.6%). White solid; m. p. 107–108 °C. ^{1}H NMR (300 MHz, DMSO) δ 9.07 (d, *J* = 5.40 Hz, 1H), 8.28–8.23 (m, 1H), 7.83–7.73 (m, 2H), 7.49–7.43 (m, 1H), 7.03 (t, *J* = 9.00 Hz, 1H), 2.56 (s, 3H). ^{13}C NMR (75 MHz, DMSO) δ 166.80, 161.69, 147.64, 147.58, 135.17, 135.11, 125.68, 125.66, 124.03, 123.94, 120.23, 119.69, 119.45, 118.07, 117.80, 117.74, 116.07, 115.75, 42.22, 42.14. HRMS (ESI): calcd for $C_{14}H_{10}F_2N_3O$ [M + H]$^+$ 274.07864, found 274.08060. HPLC (80% methanol in water): t_R = 11.26 min, 96.62%.

*4.2.3.9. 5-(3,4-difluorophenyl)-3-(6-methylpyridin-3-yl)-1,2,4-oxadiazole (**25**).* Yield: 0.325 g (45.1%). White solid; m. p. 244–245 °C. ^{1}H NMR (300 MHz, DMSO) δ 9.09 (s, 1H), 8.28 (d, *J* = 7.92 Hz, 1H), 7.88–7.85 (m, 2H), 7.73–7.67 (m, 1H), 7.49–7.46 (m, 1H), 2.56 (s, 3H). ^{13}C NMR (75 MHz, DMSO) δ 168.24, 165.82, 165.65, 163.11, 162.53, 162.35, 148.68, 136.23, 127.45, 125.07, 120.74, 113.17, 113.04, 112.92, 112.79, 110.77, 110.43, 110.09, 25.59. HRMS (ESI): calcd for $C_{14}H_{10}F_2N_3O$ [M + H]$^+$ 274.07864, found 274.07934. HPLC (80% methanol in water): t_R = 10.47 min, 97.53%.

*4.2.3.10. 5-(3,4-difluorophenyl)-3-(4-methylpyridin-2-yl)-1,2,4-oxadiazole (**26**).* Yield: 0.34 g (47.2%). White solid; m. p. 148–149 °C. ^{1}H NMR (300 MHz, DMSO) δ 8.63 (d, *J* = 4.47 Hz, 1H), 8.00 (s, 1H), 7.89 (d, *J* = 4.83 Hz, 2H), 7.74–7.68 (m, 2H), 7.46 (d, *J* = 3.66 Hz, 2H), 2.45 (s, 3H). ^{13}C NMR (75 MHz, DMSO) δ 165.79, 165.62, 162.49, 162.32, 161.08, 147.73, 147.66, 129.66, 129.60, 127.01, 126.77, 113.05, 112.92, 112.81, 112.68, 110.72, 110.37, 110.03, 15.69. HRMS (ESI): calcd for $C_{14}H_9F_2N_3ONa$ [M + Na]$^+$ 300.03552, found 300.03671. HPLC (80% methanol in water): t_R = 10.93 min, 99.13%.

*4.2.3.11. 5-(3,4-difluorophenyl)-3-(1H-indol-4-yl)-1,2,4-oxadiazole (**27**).* Yield: 0.34 g (53.1%). White solid; m. p. 229–230 °C. ^{1}H NMR (300 MHz, DMSO) δ 11.52 (s, 1H), 8.26 (t, *J* = 8.46 Hz, 1H), 8.10–8.08 (m, 1H), 7.93–7.56 (m, 4H), 7.32–7.26 (m, 1H), 7.08 (s, 1H). ^{13}C NMR (75 MHz, DMSO) δ 170.55, 165.81, 165.63, 162.51, 162.34, 137.91, 128.78, 125.88, 122.31, 122.15, 121.63, 116.68, 112.99, 112.86, 112.75, 112.62, 110.39, 110.05, 109.71, 103.61, 100.75. HRMS (ESI): calcd for $C_{16}H_{10}F_2N_3O$ [M + H]$^+$ 298.07864, found 298.07909. HPLC (80% methanol in water): t_R = 10.72 min, 98.91%.

*4.2.3.12. 5-(3,4-difluorophenyl)-3-(naphthalen-2-yl)-1,2,4-oxadiazole (**28**).* Yield: 0.293 g (44.2%). White solid; m. p. 207–208 °C. ^{1}H NMR (300 MHz, DMSO) δ 8.56–8.49 (m, 1H), 8.22–7.96 (m, 4H), 7.70–7.55 (m, 2H), 7.36 (m, 1H), 7.27 (m, 1H), 7.07 (m, 1H). HRMS (ESI): calcd for $C_{18}H_{10}F_2N_2O$ [M + H]$^+$ 309.29905, found 309.29987. HPLC (80% methanol in water): t_R = 11.54 min, 98.71%.

*4.2.3.13. 5-(3,4-difluorophenyl)-3-([1,1′-biphenyl]-4-yl)-1,2,4-oxadiazole (**29**).* Yield: 0.313 g (43.2%). White solid; m. p. 151–152 °C. ^{1}H NMR (300 MHz, DMSO) δ 8.19–8.13 (m, 2H), 8.02–7.87 (m, 4H), 7.76–7.67 (m, 3H), 7.53–7.17 (m, 3H). ^{13}C NMR (75 MHz, DMSO) δ 168.08, 164.27, 164.10, 160.98, 160.81, 143.16, 138.78, 128.87, 128.04, 127.56, 127.26, 126.63, 126.22, 126.07, 124.53, 117.92, 111.47, 111.35, 111.23, 111.10, 109.02, 108.68, 108.34. HRMS (ESI): calcd for $C_{20}H_{13}F_2N_2O$ [M + H]$^+$ 335.09905, found 335.09987. HPLC (80% methanol in water): t_R = 12.54 min, 96.29%.

*4.2.3.14. 5-(3,4-difluorophenyl)-3-(2-fluorophenyl)-1,2,4-oxadiazole (**30**).* Yield: 0.365 g (50.6%). White solid; m. p. 135–136 °C. ^{1}H NMR (300 MHz, DMSO) δ 8.66 (d, *J* = 4.14 Hz, 1H), 8.04–7.98 (m, 1H), 7.88–7.73 (m, 3H), 7.08 (t, *J* = 8.99 Hz, 2H). ^{13}C NMR (75 MHz, DMSO) δ 165.65, 165.58, 162.00, 158.61, 154.81, 154.65, 151.96, 151.79, 151.44, 151.28, 148.67, 148.49, 134.23, 134.11, 131.04, 131.02, 126.40, 126.35, 126.29, 126.24, 125.54, 125.50, 119.69, 119.45, 118.03, 117.77, 117.40, 117.13. HRMS (ESI): calcd for $C_{14}H_8F_3N_2O$ [M + H]$^+$ 277.05832, found 277.05884. HPLC (80% methanol in water): t_R = 9.53 min, 97.97%.

*4.2.3.15. 5-(3,4-difluorophenyl)-3-(3-fluorophenyl)-1,2,4-oxadiazole (**31**).* Yield: 0.324 g (45.0%). White solid; m. p. 162–163 °C. ^{1}H NMR (300 MHz, DMSO) δ 8.28–8.13 (m, 2H), 8.00–7.93 (m, 1H), 7.88–7.76 (m, 1H), 7.72–7.63 (m, 1H), 7.53–7.47 (m, 1H), 7.20 (s, 1H). ^{13}C NMR (75 MHz, DMSO) δ 164.36, 161.11, 155.92, 152.60, 137.79, 137.72, 132.18, 132.07, 130.19, 126.60, 125.75, 125.70, 123.81, 123.77, 120.23, 120.19, 119.35, 119.07, 117.37, 117.06, 114.41, 114.10. HRMS (ESI): calcd for $C_{14}H_8F_3N_2O$ [M + H]$^+$ 277.05832, found 277.05884. HPLC (80% methanol in water): t_R = 10.26 min, 98.19%.

*4.2.3.16. 5-(3,4-difluorophenyl)-3-(4-fluorophenyl)-1,2,4-oxadiazole (**32**).* Yield: 0.353 g (49.0%). White solid; m. p. 140–141 °C. ^{1}H NMR (300 MHz, DMSO) δ 8.26–8.20 (m, 1H), 8.19–8.06 (m, 3H), 7.85–7.70 (m, 1H), 7.51–7.38 (m, 2H). ^{13}C NMR (75 MHz, DMSO) δ 161.99, 158.60, 154.81, 154.64, 151.96, 151.78, 151.44, 151.28, 134.24, 134.13, 131.04, 131.02, 126.41, 126.36, 126.30, 126.25, 125.56, 125.51, 119.70, 119.46, 118.04, 117.78, 117.41, 117.14. HRMS (ESI): calcd for $C_{14}H_8F_3N_2O$ [M + H]$^+$ 277.05832, found 277.05884. HPLC (80% methanol in water): t_R = 10.47 min, 98.54%.

*4.2.3.17. 5-(3,4-difluorophenyl)-3-(4-chlorophenyl)-1,2,4-oxadiazole (**33**).* Yield: 0.334 g (48.6%). White solid; m. p. 243–244 °C. ^{1}H NMR (300 MHz, DMSO) δ 8.26–8.20 (m, 1H), 8.19–8.06 (m, 3H), 7.85–7.70 (m, 1H), 7.51–7.38 (m, 2H). HRMS (ESI): calcd for $C_{14}H_7ClF_2N_2O$ [M + H]$^+$ 293.67832, found 293.67884. HPLC (80% methanol in water): t_R = 13.47 min, 98.84%.

*4.2.3.18. 5-(3,4-difluorophenyl)-3-(2-bromophenyl)-1,2,4-oxadiazole (**34**).* Yield: 0.302 g (47.9%). White solid; m. p. 187–188 °C. ^{1}H NMR (300 MHz, DMSO) δ 8.30–8.14 (m, 2H), 8.02–7.87 (m, 2H), 7.73 (s, 1H), 7.65–7.53 (m, 2H). HRMS (ESI): calcd for $C_{14}H_6BrF_2N_2O$ [M - H]$^-$ 334.96371, found 334.96375. HPLC (80% methanol in water): t_R = 10.19 min, 98.43%.

*4.2.3.19. 5-(3,4-difluorophenyl)-3-(4-bromophenyl)-1,2,4-oxadiazole (**35**).* Yield: 0.343 g (54.4%). White solid; m. p. 131–132 °C. ^{1}H NMR (300 MHz, DMSO) δ 8.25–28.21 (m, 1H), 8.15–28.99 (m, 3H), 7.82–28.72 (m, 3H), ^{13}C NMR (75 MHz, DMSO) δ 168.66, 165.28, 165.63, 162.51, 162.33, 136.00, 132.95, 130.91, 129.29, 127.45, 127.21, 123.75, 113.11, 112.98, 112.86, 112.74, 110.76, 110.42, 110.08. HRMS (ESI): calcd for $C_{14}H_6BrF_2N_2O$ [M - H]$^-$ 334.96371, found 334.96375. HPLC (80% methanol in water): t_R = 9.28 min, 97.91%.

*4.2.3.20. 3,5-bis(3,4-difluorophenyl)-1,2,4-oxadiazole (**36**).* Yield: 0.298 g (43.8%). White solid; m. p. 207–208 °C. ^{1}H NMR (300 MHz, DMSO) δ 7.92 (d, *J* = 5.52 Hz, 2H), 7.77–7.74 (m, 3H), 7.72–7.54 (m, 1H). ^{13}C NMR (75 MHz, DMSO) δ 154.90, 151.32, 130.73, 130.69, 124.47, 124.42, 124.38, 124.33, 120.25, 119.97, 118.58, 118.58, 118.23, 118.00, 117.45, 117.43, 116.70, 116.44. HRMS (ESI): calcd for $C_{14}H_6F_4N_2O$ [M + H]$^+$ 295.21371, found 295.21375. HPLC (80% methanol in water): t_R = 9.34 min, 96.91%.

*4.2.3.21. 5-(3,4-difluorophenyl)-3-(4-acetyl phenyl)-1,2,4-oxadiazole (**37**).* Yield: 0.302 g (44.8%). White solid; m. p. 230–231 °C. ^{1}H NMR (300 MHz, DMSO) δ 8.07 (d, J = 8.34 Hz, 2H), 7.87–7.84 (m, 4H), 7.72–7.66 (m, 1H), 2.19 (s, 3H). ^{13}C NMR (75 MHz, DMSO) δ 174.81, 169.47, 165.76, 165.59, 162.47, 162.30, 153.60, 141.36, 128.91, 128.48, 127.58, 126.95, 126.63, 112.95, 112.83, 112.71, 112.58, 110.56, 110.22, 109.88, 12.65. HRMS (ESI): calcd for $C_{16}H_9F_2N_2O_2$ $[M - H]^-$ 299.06376, found 299.06550. HPLC (80% methanol in water): t_R = 10.34 min, 97.65%.

*4.2.3.22. 5-(3,4-difluorophenyl)-3-(p-tolyl)-1,2,4-oxadiazole (**38**).* Yield: 0.356 g (49.4%). White solid; m. p. 150–151 °C. ^{1}H NMR (300 MHz, DMSO) δ 8.09–7.86 (m, 4H), 7.84–7.81 (m, 1H), 7.76–7.66 (m, 2H), 2.59 (s, 3H). ^{13}C NMR (75 MHz, DMSO) δ 169.85, 165.82, 165.64, 162.36, 143.24, 137.37, 131.81, 131.21, 128.47, 124.41, 119.48, 116.65, 113.00, 112.88, 112.76, 112.63, 110.52, 110.18, 109.83, 22.47. HRMS (ESI): calcd for $C_{15}H_{11}F_2N_2O$ $[M + H]^+$ 273.0834, found 273.08384. HPLC (80% methanol in water): t_R = 9.34 min, 98.78%.

*4.2.3.23. 5-(3,4-difluorophenyl)-3-(3-methoxyphenyl)-1,2,4-oxadiazole (**39**).* Yield: 0.401 g (57.8%). White solid; m. p. 122–123 °C. ^{1}H NMR (300 MHz, DMSO) δ 7.88 (s, 2H), 7.82–7.45 (m, 4H), 7.21–7.19 (m, 1H), 3.86 (s, 3H). ^{13}C NMR (75 MHz, DMSO) δ 169.74, 165.81, 165.64, 162.51, 162.34, 161.08, 131.88, 128.39, 120.80, 119.04, 113.53, 112.99, 112.86, 112.74, 112.62, 110.54, 110.20, 109.85, 56.76. HRMS (ESI): calcd for $C_{15}H_{11}F_2N_2O_2$ $[M + H]^+$ 289.07831, found 289.0786. HPLC (80% methanol in water): t_R = 8.79 min, 98.31%.

*4.2.3.24. 3-(4-(tert-butyl)phenyl)-5-(3,4-difluorophenyl)-1,2,4-oxadiazole (**40**).* Yield: 0.386 g (59.1%). White solid; m. p. 110–111 °C. ^{1}H NMR (300 MHz, DMSO) δ 7.99 (d, J = 8.31 Hz, 2H), 7.85 (d, J = 5.55 Hz, 2H), 7.69–7.59 (m, 3H), 1.32 (s, 9H). ^{13}C NMR (75 MHz, DMSO) δ 169.74, 165.80, 165.62, 162.50, 162.33, 156.11, 128.69, 128.35, 127.63, 127.46, 126.27, 124.39, 113.00, 112.88, 112.76, 112.63, 110.56, 110.22, 109.88, 36.15, 32.32, 32.24, 32.13. HRMS (ESI): calcd for $C_{18}H_{17}F_2N_2O$ $[M + H]^+$ 315.13035, found 315.1312. HPLC (80% methanol in water): t_R = 8.98 min, 97.10%.

*4.2.3.25. 5-(3,4-difluorophenyl)-3-(3,5-dimethoxyphenyl)-1,2,4-oxadiazole (**41**).* Yield: 0.341 g (52.4%). White solid; m. p. 123–124 °C. ^{1}H NMR (300 MHz, DMSO) δ 8.22–7.94 (m, 2H), 7.76–7.70 (m, 1H), 7.19–7.15 (m, 2H), 6.72 (s, 3H), 3.83 (s, 6H). ^{13}C NMR (75 MHz, DMSO) δ 168.60, 161.34, 154.74, 154.58, 151.92, 151.74, 151.38, 151.21, 148.63, 148.45, 127.99, 126.32, 126.28, 126.22, 126.17, 119.61, 119.37, 117.97, 117.71, 116.00, 115.67, 105.30, 103.96, 42.20, 42.12. HRMS (ESI): calcd for $C_{16}H_{13}F_2N_2O_3$ $[M + H]^+$ 319.08888, found 319.08992. HPLC (80% methanol in water): t_R = 9.34 min, 95.91%.

4.3. Pharmacology

4.3.1. Cell culture conditions

HepG2 cells stably transfected with an ARE luciferase reporter (HepG2-ARE-C8) were kindly provided by Professor A. N. Tony Kong (Rutgers University, Piscataway, NJ) and Prof. Rong Hu (China Pharmaceutical University). Cells were cultured in DMEM (Gibco, USA) with 10% (v/v) fetal bovine serum (FBS, Gibco, USA) in a humidified atmosphere of 5% CO_2 and 95% air at 37 °C. L02 cells (Cell Bank of Shanghai Institute of Biochemistry and Cell Biology, Shanghai Institutes for Biological Sciences, Chinese Academy of Sciences) were cultured in DMEM (Gibco, USA) supplemented with 10% (v/v) FBS in a humidified atmosphere of 5% CO_2 and 95% air at 37 °C.

4.3.2. Compound dilutions

All compounds were dissolved in DMSO at 10 mmol per liter as stock solutions and stored at −20 °C. Fresh cell-culture medium was used to dilute the stock solutions.

4.3.3. MTT analysis

Cytotoxicity was determined using the MTT assay. MTT was purchased from Sigma (St. Louis, MO). It was dissolved in phosphate-buffered saline (PBS) at a concentration of 5 mg/mL as the stock solution and stored at −20 °C. After the cells were treated with a density gradient of test compounds or DMSO for 24 h, 20.0 μL of MTT solution (5 mg/mL) was added to each well of a 96-well plate for 4 h. Next, the solution was removed, and 150.0 μL of DMSO was added to each well to dissolve the water-soluble MTT-formazan crystals. The absorbance values (OD value) were recorded at 570 nm by an Elx800 absorbance microplate reader (BioTek, Vermont, USA).

$$IC_{50} = [1 - (OD_{test} - OD_{blank}) / (OD_{control} - OD_{blank})]*100\%$$

4.3.4. ARE-luciferase activity assay

The experimental procedures were performed as reported previously [35]. HepG2-ARE-C8 cells stably expressing ARE-luciferase were seeded onto 48-well plates at a density of 5×10^4 cells/well and incubated overnight before incubation with test compounds. The cells were treated with different concentrations of the test compounds, with *t*BHQ serving as the positive control, DMSO serving as the negative control, and the luciferase cell culture lysis reagent serving as the blank. After 24 h of treatment, the medium was removed and 400.0 μL of cold PBS was added to each well. Next, the cells were lysed in the luciferase cell culture lysis reagent. After centrifugation, 20.0 μL of the supernatant was used for determining the luciferase activity according to the protocol provided by the manufacturer (Promega, Madison, WI). The luciferase activity was measured by a Luminoskan Ascent luminometer (Thermo Scientific, USA). The data were obtained in triplicates and expressed as fold induction over control.

$$\text{Inductivity} = (\text{RLUtest} - \text{RLUblank})/(\text{RLUcontrol} - \text{RLUblank})$$

RLU = relative light unit

4.3.5. Western blotting

Anti-NQO1 (sc-271116) antibodies were obtained from Santa Cruz Biotechnology (Santa Cruz, CA, USA). Anti-β-actin (AP0060) and anti-Nrf2 (BS1258) were purchased from Bioworlde (Bioworlde, USA). Anti-HO-1 (no. 5853 S) was purchased from Cell Signaling Technology (USA). The cells were washed once with ice-cold PBS and dissociated with 1 mL of 1 × trypsin. The cells were centrifuged at 2000 rpm and lysed in 80.0 μL of lysis buffer, which contained 150.0 mM NaCl, 1% NP-40, 50.0 mM Tris-HCl, pH 7.5, 1 mM NaF, EDTA, DTT, Leu, and PMSF for 1 h. The cells were centrifuged again at 12000 rpm for 20 min at 4 °C. The supernatants were collected, and the protein concentrations of the whole cell lysates were determined by the BCA assay with Varioskan Flash (Thermo, Waltham, MA) at 562 nm. The samples were stored at −80 °C until use. The Nuclear-Cytosol Extraction Kit (KeyGEN, NJ, China) was used to isolate the nuclear and cytosolic protein according to the protocol. The collected proteins were stored at −80 °C until use.

Equal amounts of total protein extracts were separated by SDS-

PAGE and then electroblotted onto PVDF membranes (PerkinElmer, Northwalk, CT, USA). After blocking with 1% BSA for 1 h, the membranes were incubated at 37 °C for 1 h and then at 4 °C overnight with a primary antibody. They were treated with a DyLight 800 labeled secondary antibody at 37 °C for 1 h. The membranes were screened with the Odyssey infrared imaging system (LI-COR, Lincoln, Nebraska, USA).

4.3.6. Immunofluorescence of L02 cells

L02 cells were grown on coverslips for 24 h then treated with compounds at different concentrations for 12 h. The cells were fixed and probed with an Nrf2 antibody and an DyLight 488-labeled anti-rabbit IgG antibody (Santa Cruz Biotechnology, Santa Cruz, CA), before being stained with the fluorochrome dye DAPI (Santa Cruz Biotechnology, Santa Cruz, CA) to visualize the nuclei observed under a laser scanning confocal microscope (Olympus Fluoview FV1000, Japan) with peak excitation wavelengths of 570 and 340 nm.

4.3.7. qRT-PCR

Total RNA of the L02 cells was isolated using TRIzol (Invitrogen). The quantification and purity of the RNA samples were assessed by A260/A280 absorption, and RNA samples with ratios above 1.8 were stored at −80 °C for further analysis. The RNA was reverse transcribed using the PrimeScript RT reagent kit following the manufacturer's instructions. The following primer sequences were used, Nrf2 sense primer 5′-AACCACCCTGAAAGCACGC-3′ and antisense primer 5′-TGAAATGCCGGAGTCAGAATC-3'; HO-1 sense primer 5′- ATGGCCTCCCTGTACCACATC-3′ and antisense primer 5′- TGTTGCGCTCAATCTCCTCCT-3'; NQO-1 sense primer 5′-CGCAGACCTTGTGATATTCCAG-3′ and antisense primer 5′-CGTTTCTTCCATCCTTCCAGG-3'; GCLM sense primer 5′-TTGGAGTTGCACAGCTGGATTC-3′ and antisense primer 5′-TGGTTTTACCTGTGCCCACTG-3'; GCLC sense primer: 5′-GTCCTCAGGTGACATTCCAAGC-3'; and antisense primer: 5′-TGTTCTTCAGGGGCTCCAGTC-3'. GAPDH was used as the internal controls (sense primer 5′-AGGTCGGTGTGAACGGATTTG-3′ and antisense primer 5′-TGTAGACCATGTAGTTGAGGTCA-3′). Quantitative real-time RT-PCR analysis of Nrf2, NQO1, HO-1, and GCLM were performed using a STEPONE SYSTERM Fast Real Time PCR system (Applied Biosystems). GAPDH was used for normalization. The values are expressed as the fold increase compared with the control. Each cycle consisted of denaturation at 95 °C for 5 s combined with annealing and extension at 60 °C for 30 s. A total of 40 cycles were performed.

4.3.8. Transfection of small interfering RNA (siRNA)

A predesigned siRNA against human Nrf2 (catalog no. 115762) and a control scrambled siRNA (catalog no. 4611) were purchased from Biomics (Biomics, China). L02 cells were plated at a density of 7×10^5 cells per 60 mm dish. The cells were transfected with 50 nM siRNA against Nrf2 using Lipofectamine 2000 (Invitrogen). After 24 h incubation, fresh medium was added, and the cells were cultured for another 48 h. The cells were then treated with 20.0 compound **25** for an additional 12 h and lysed for qRT-PCR.

4.3.9. Statistical analysis

Statistical analyses were calculated using both one-way ANOVA and Kruskal-Wallis tests for the multiple comparision. For all tests only P values < 0.05 were considered statistically significant. All descriptive data are reported as the mean ± SD. GraphPad Prism was used for statistical analysis.

4.3.10. Animals and experimental design

Animal studies were conducted according to protocols approved by the Institutional Animal Care and Use Committee of China Pharmaceutical University. All animals were appropriately used in a scientifically valid and ethical manner. The animal use approval number of China Pharmaceutical University is SYXK(苏)2016-0011. The animal room was environmentally controlled at 25 °C, 55%–60% humidity and 12 h light/dark cycle. 50 female C57BL/6 mice (20–25 g) were randomly divided into five groups (n = 10): Group I (control group) received normal saline as a vehicle for 7 days. Group II mice (APAP group) were injected with APAP (Sigma-Aldrich, St. Louis no. 103-90-2) on the 7th day with a single dose of 300 mg/kg. Groups III-V mice (**25** + APAP group) were injected with compound **25** at a low-dose (10 mg/kg/day) group, middle-dose (50 mg/kg/day) group, and a high-dose (100 mg/kg/day) for 7 consecutive days. One hour after the last administration, a single dose of APAP (300 mg/kg) was injected to the mice of groups III-V. Both compound **25** and APAP were dissolved in physiological saline. The injection volume was calculated from the body weight of the mice and should not exceed 200 μL. After 24 h of the APAP challenge, all mice were sacrificed to obtain blood and liver samples for further biochemical analysis.

4.3.11. Measurement of plasma ALT and AST levels

Blood samples from mice were centrifuged at 3000×g, for 10 min at 4 °C to obtain the serum supernatants. The contents of ALT and AST in serum were measured using commercially available kits (Nanjing Jiancheng Institute of Biotechnology, China).

4.3.12. Assay for antioxidant enzymes activity

Liver tissues were collected and homogenized in phosphate buffer (pH 7.0). Tissue homogenates were then centrifuged at 10,000×g, for 10 min at 4 °C to separately obtain the supernatant and pellet for further experiments. The protein concentration was determined using a BCA protein assay kit (Pierce, Rockford, IL, USA).

4.3.13. Measurement of hepatic GSH levels

The GSH level was measured using a modified protocol with a GSH kit provided by Jiancheng Bioengineering Institute (Nanjing, China). The observation absorbance of the reaction was read at 420 nm and the enzyme activity was calculated as μmol/g protein.

4.3.14. Measurement of hepatic superoxide dismutase (SOD) activity

SOD activity was determined by measuring the ability of SOD to inhibit the photochemical reduction of nitro blue tetrazolium (NBT) according to the absorbance at 550 nm. Using the commercial kit protocol provided by Jiancheng Bioengineering Institute (Nanjing, China), the data were expressed as SOD U/mg protein compared with the standard.

4.3.15. GST activity assay

The GST level was determined by a commercial kit provided by Jiancheng Bioengineering Institute (Nanjing, China). The observation absorbance of the reaction was read at 412 nm, and the activity was calculated as U/mg protein. GSH consumption was used as a marker to evaluate whether APAP was a substrate for GST.

Ancillary information

Author contributions

The manuscript was written with contributions from all authors. All authors have given approved the final version of the manuscript.

Notes

The authors declare no competing financial interest.

Acknowledgement

This study was supported by projects, [81602948], [81773581] and [81773639] of the National Natural Science Foundation of China, the Natural Science Foundation of Jiangsu Province of China [no. BK20160746]; [2015ZX09101032], [2017ZX09302003] and [2018ZX09711002-003-006] of the National Major Science and Technology Project of China (Innovation and Development of New Drugs); the Priority Academic Program Development of Jiangsu Higher Education Institutions; the College Students Innovation Project for the R&D of Novel Drugs [J1310032]; the China Post-doctoral Science Foundation-funded project [2017M620232]; The Program for Outstanding Scientific and Technological Innovation Team of Jiangsu Higher Education [YY20180315004]; and Fundamental Research Funds for the Central Universities [2016ZPT005].

Abbreviations

Keap1	Kelch-like ECH-associated protein-1
Nrf2	nuclear factor erythroid 2-related factor 2
ARE	antioxidant response element
b-ZIP	basic-leucine zipper
ROS	reactive oxygen species
NQO1	NAD(P)H/quinone oxidoreductase
HO-1	heme oxygenase-1
SAR	structure-activity relationship
OTC	over-the-counter
APAP	acetaminophen
GSH	glutathione
HCC	hepatocellular carcinoma
DMF	dimethyl fumarate
tBHQ	tertiary butylhydroquinone
MAPK	mitogen-activated protein kinases
PI3K	phosphoinositide 3-kinase
P38	p38 MAP kinase
JNK	c-Jun N-terminal kinase
UPLC-MS/MS	ultra-performance liquid chromatography-tandem mass spectrometry
NBT	nitro blue tetrazolium
CYP450	cytochrome p450
NAPQI	n-acetyl-para-benzoquinone imine
GCLC	cysteine ligase catalytic subunit
GCLM	cysteine ligase regulatory subunit

Appendix A. Supplementary data

Supplementary data related to this article can be found at https://doi.org/10.1016/j.ejmech.2018.08.071.

References

[1] L. Baird, A.T. Dinkova-Kostova, The cytoprotective role of the Keap1-Nrf2 pathway, Arch. Toxicol. 85 (2011) 241–272.
[2] T.W. Kensler, N. Wakabayashi, S. Biswal, Cell survival responses to environmental stresses via the Keap1-Nrf2-ARE pathway, Annu. Rev. Pharmacol. Toxicol. 47 (2007) 89–116.
[3] L.G. Higgins, J.D. Hayes, The cap'n'collar transcription factor Nrf2 mediates both intrinsic resistance to environmental stressors and an adaptive response elicited by chemopreventive agents that determines susceptibility to electrophilic xenobiotics, Chem. Biol. Interact. 192 (2011) 37–45.
[4] R. Hu, C.L. Saw, R. Yu, A.N. Tony Kong, Regulation of NF-E2-related factor 2 signaling for cancer chemoprevention: antioxidant coupled with antiinflammatory, Antioxidants Redox Signal. 13 (2010) 1679–1698.
[5] J.D. Hayes, A.T. Dinkova-Kostova, The Nrf2 regulatory network provides an interface between redox and intermediary metabolism, Trends Biochem. Sci. 39 (2014) 199–218.
[6] H.K. Bryan, A. Olayanju, C.E. Goldring, B.K. Park, The Nrf2 cell defence pathway: Keap1-dependent and -independent mechanisms of regulation, Biochem. Pharmacol. 85 (2013) 705–717.
[7] D.D. Zhang, The nrf2-Keap1-are signaling pathway: the regulation and dual function of Nrf2 in cancer, Antioxidants Redox Signal. 13 (2010) 1623–1626.
[8] S.K. Niture, R. Khatri, A.K. Jaiswal, Regulation of nrf2-an update, Free Radic. Biol. Med. 66 (2014) 36–44.
[9] Z.Y. Jiang, M.C. Lu, Q.D. You, Discovery and development of kelch-like ECH-associated protein 1. Nuclear factor erythroid 2-related factor 2 (KEAP1:NRF2) protein-protein interaction inhibitors: achievements, challenges, and future directions, J. Med. Chem. 59 (2016) 10837–10858.
[10] D.D. Zhang, Bardoxolone brings nrf2-based therapies to light, Antioxidants Redox Signal. 19 (2013) 517–518.
[11] F. Hong, K.R. Sekhar, M.L. Freeman, D.C. Liebler, Specific patterns of electrophile adduction trigger Keap1 ubiquitination and Nrf2 activation, J. Biol. Chem. 280 (2005) 31768–31775.
[12] A. Uruno, H. Motohashi, The Keap1-Nrf2 system as an in vivo sensor for electrophiles, Nitric Oxide 25 (2011) 153–160.
[13] J.W. Kaspar, S.K. Niture, A.K. Jaiswal, Nrf2: INrf2 (Keap1) signaling in oxidative stress, Free Radic. Biol. Med. 47 (2009) 1304–1309.
[14] H. Motohashi, F. Katsuoka, J.D. Engel, M. Yamamoto, Small Maf proteins serve as transcriptional cofactors for keratinocyte differentiation in the Keap1–Nrf2 regulatory pathway, Proc. Natl. Acad. Sci. U.S.A. 101 (2004) 6379–6384.
[15] D.J. Reuland, S. Khademi, C.J. Castle, D.C. Irwin, J.M. McCord, B.F. Miller, K.L. Hamilton, Upregulation of phase II enzymes through phytochemical activation of Nrf2 protects cardiomyocytes against oxidant stress, Free Radic. Biol. Med. 56 (2013) 102–111.
[16] C. Tonelli, I.I.C. Chio, D.A. Tuveson, Transcriptional regulation by Nrf2, Antioxidants Redox Signal. 7342 (2017) 1–19.
[17] W. Tang, Y.F. Jiang, M. Ponnusamy, M. Diallo, Role of Nrf2 in chronic liver disease, World J. Gastroenterol. 20 (2014) 13079–13087.
[18] X. Chen, J. Liu, S.Y. Chen, Sulforaphane protects against ethanol-induced oxidative stress and apoptosis in neural crest cells by the induction of Nrf2-mediated antioxidant response, Br. J. Pharmacol. 169 (2013) 437–448.
[19] W. Wang, Y. He, G. Yu, B. Li, D.W. Sexton, T. Wileman, A.A. Roberts, C.J. Hamilton, R. Liu, Y. Chao, Y. Shan, Y. Bao, Sulforaphane protects the liver against CdSe quantum dot-induced cytotoxicity, PLoS One 10 (2015), e0138771.
[20] L. Wang, S. Zhang, H. Cheng, H. Lv, G. Cheng, X. Ci, Nrf2-mediated liver protection by esculentoside A against acetaminophen toxicity through the AMPK/Akt/GSK3beta pathway, Free Radic. Biol. Med. 101 (2016) 401–412.
[21] J.A. Morales-Gonzalez, E. Madrigal-Santillan, A. Morales-Gonzalez, M. Bautista, E. Gayosso-Islas, C. Sanchez-Moreno, What is known regarding the participation of factor Nrf-2 in liver regeneration? Cells 4 (2015) 169–177.
[22] I.M. Copple, C.E. Goldring, N.R. Kitteringham, B.K. Park, The Nrf2–Keap1 defence pathway: role in protection against drug-induced toxicity, Toxicology 246 (2008) 24–33.
[23] N.R. Kitteringham, A. Abdullah, J. Walsh, L. Randle, R.E. Jenkins, R. Sison, C.E. Goldring, H. Powell, C. Sanderson, S. Williams, L. Higgins, M. Yamamoto, J. Hayes, B.K. Park, Proteomic analysis of Nrf2 deficient transgenic mice reveals cellular defence and lipid metabolism as primary Nrf2-dependent pathways in the liver, J. Proteomics 73 (2010) 1612–1631.
[24] M.S. Yates, Q.T. Tran, P.M. Dolan, W.O. Osburn, S. Shin, C.C. McCulloch, J.B. Silkworth, K. Taguchi, M. Yamamoto, C.R. Williams, K.T. Liby, M.B. Sporn, T.R. Sutter, T.W. Kensler, Genetic versus chemoprotective activation of Nrf2 signaling: overlapping yet distinct gene expression profiles between Keap1 knockout and triterpenoid-treated mice, Carcinogenesis 30 (2009) 1024–1031.
[25] J. Liu, K.C. Wu, Y.F. Lu, E. Ekuase, C.D. Klaassen, Nrf2 protection against liver injury produced by various hepatotoxicants, Oxid. Med. Cell. Longev. 2013 (2013) 305861.
[26] B. Sid, C. Glorieux, M. Valenzuela, G. Rommelaere, M. Najimi, N. Dejeans, P. Renard, J. Verrax, P.B. Calderon, AICAR induces Nrf2 activation by an AMPK-independent mechanism in hepatocarcinoma cells, Biochem. Pharmacol. 91 (2014) 168–180.
[27] J.R. Mitchell, D.J. Jollow, W.Z. Potter, J.R. Gillette, B.B. Brodie, Acetaminophen-induced hepatic necrosis. IV. Protective role of glutathione, J. Pharmacol. Exp. Therapeut. 187 (1973) 211–217.
[28] H. Jaeschke, T. Knight, M.L. Bajt, The role of oxidant stress and reactive nitrogen species in acetaminophen hepatotoxicity, Toxicol. Lett. 144 (2003) 279–288.
[29] I.M. Copple, C.E. Goldring, R.E. Jenkins, et al., The hepatotoxic metabolite of acetaminophen directly activates the Keap1-Nrf2 cell defense system, Hepatology 48 (2008) 1292–1301.
[30] C.E. Goldring, N.R. Kitteringham, R. Elsby, et al., Activation of hepatic Nrf2 in vivo by acetaminophen in CD-1 mice, Hepatology 39 (2004) 1267–1276.
[31] A.J. Chia, C.E. Goldring, N.R. Kitteringham, et al., Differential effect of covalent protein modification and glutathione depletion on the transcriptional response of Nrf2 and NF-kappaB, Biochem. Pharmacol. 80 (2010) 410–421.
[32] L.L. Xu, J.F. Zhu, X.L. Xu, J. Zhu, L. Li, M.Y. Xi, Z.Y. Jiang, M.Y. Zhang, F. Liu, M.C. Lu, Q.C. Bao, Q. Li, C. Zhang, J.L. Wei, X.J. Zhang, L.S. Zhang, Q.D. You, H.P. Sun, Discovery and modification of in vivo active Nrf2 activators with 1,2,4-oxadiazole core: hits identification and structure-activity relationship

study, J. Med. Chem. 58 (2015) 5419–5436.
[33] R.H. Scannevin, S. Chollate, M.Y. Jung, M. Shackett, H. Patel, P. Bista, W. Zeng, S. Ryan, M. Yamamoto, M. Lukashev, K.J. Rhodes, Fumarates promote cytoprotection of central nervous system cells against oxidative stress via the nuclear factor (erythroid-derived 2)-like 2 pathway, J. Pharmacol. Exp. Therapeut. 341 (2012) 274–284.
[34] S. Magesh, Y. Chen, L. Hu, Small molecule modulators of Keap1-Nrf2-ARE pathway as potential preventive and therapeutic agents, Med. Res. Rev. 32 (2012) 687–726.
[35] M. Kobayashi, M. Yamamoto, Nrf2-Keap1 regulation of cellular defense mechanisms against electrophiles and reactive oxygen species, Adv. Enzym. Regul. 46 (2006) 113–140.
[36] S. Singh, S. Vrishni, B.K. Singh, I. Rahman, P. Kakkar, Nrf2-ARE stress response mechanism: a control point in oxidative stress-mediated dysfunctions and chronic inflammatory diseases, Free Radic. Res. 44 (2010) 1267–1288.
[37] J. Kim, Y.N. Cha, Y.J. Surh, A protective role of nuclear factor-erythroid 2-related factor-2 (Nrf2) in inflammatory disorders, Mutat. Res. 690 (2010) 12–23.
[38] M.C. Lu, J.A. Ji, Z.Y. Jiang, Q.D. You, The Keap1–nrf2–are pathway as a potential preventive and therapeutic target: an update, Med. Res. Rev. 36 (2016) 924–963.
[39] H. Xue, W. Xie, Z. Jiang, M. Wang, J. Wang, H. Zhao, X. Zhang, 3,4-Dihydroxyphenylacetic acid, a microbiota-derived metabolite of quercetin, attenuates acetaminophen (APAP)-induced liver injury through activation of Nrf-2, Xenobiotica 46 (2016) 931–939.
[40] M.Y. Xi, J.M. Jia, H.P. Sun, Z.Y. Sun, J.W. Jiang, Y.J. Wang, M.Y. Zhang, J.F. Zhu, L.L. Xu, Z.Y. Jiang, X. Xue, M. Ye, X. Yang, Y. Gao, L. Tao, X.K. Guo, X.L. Xu, Q.L. Guo, X.J. Zhang, R. Hu, Q.D. You, 3-aroylmethylene-2,3,6,7-tetrahydro-1H-pyrazino[2,1-a]isoquinolin-4(11bH)-ones as potent Nrf2/ARE inducers in human cancer cells and AOM-DSS treated mice, J. Med. Chem. 56 (2013) 7925–7938.
[41] M.Y. Xi, Z.Y. Sun, H.P. Sun, J.M. Jia, Z.Y. Jiang, L. Tao, M. Ye, X. Yang, Y.J. Wang, X. Xue, J.J. Huang, Y. Gao, X.K. Guo, S.L. Zhang, Y.R. Yang, Q.L. Guo, R. Hu, Q.D. You, Synthesis and bioevaluation of a series of alpha-pyrone derivatives as potent activators of Nrf2/ARE pathway (part I), Eur. J. Med. Chem. 66 (2013) 364–371.